Friction **3**(4): 294–319 (2015)
DOI 10.1007/s40544-015-0097-z
ISSN 2223-7690
CN 10-1237/TH

REVIEW ARTICLE

From ice superlubricity to quantum friction: Electronic repulsivity and phononic elasticity

Xi ZHANG[1,*], Yongli HUANG[2], Zengsheng MA[2], Lengyuan NIU[3], Chang Qing SUN[4,*]

[1] *Institute of Nanosurface Science and Engineering, Shenzhen University, Shenzhen 518060, China*

[2] *Key Laboratory of Low-dimensional Materials and Application Technology (MOE) and School of Materials Science and Engineering, Xiangtan University, Xiangtan 411105, China*

[3] *Institute of Coordination Bond Metrology and Engineering, College of Materials Science and Engineering, China Jiliang University, Hangzhou 310018, China*

[4] *NOVITAS, School of EEE, Nanyang Technological University, 639798, Singapore*

Received: 10 September 2015 / Revised: 22 October 2015 / Accepted: 26 November 2015

Abstract: Superlubricity means non-sticky and frictionless when two bodies are set contacting motion. Although this occurrence has been extensively investigated since 1859 when Faraday firstly proposed a quasiliquid skin on ice, the mechanism behind the superlubricity remains uncertain. This report features a consistent understanding of the superlubricity pertaining to the slipperiness of ice, self-lubrication of dry solids, and aqueous lubricancy from the perspective of skin bond-electron-phonon adaptive relaxation. The presence of nonbonding electron polarization, atomic or molecular undercoordination, and solute ionic electrification of the hydrogen bond as an addition, ensures the superlubricity. Nonbond vibration creates soft phonons of high magnitude and low frequency with extraordinary adaptivity and recoverability of deformation. Molecular undercoordination shortens the covalent bond with local charge densification, which in turn polarizes the nonbonding electrons making them localized dipoles. The locally pinned dipoles provide force opposing contact, mimicking magnetic levitation and hovercraft. O:H–O bond electrification by aqueous ions has the same effect of molecular undercoordination but it is throughout the entire body of the lubricant. Such a Coulomb repulsivity due to the negatively charged skins and elastic adaptivity due to soft nonbonding phonons of one of the contacting objects not only lowers the effective contacting force but also prevents charge from being transited between the counterparts of the contact. Consistency between theory predictions and observations evidences the validity of the proposal of interface elastic Coulomb repulsion that serves as the rule for the superlubricity of ice, wet and dry frictions, which also reconciles the superhydrophobicity, superlubricity, and supersolidity at contacts.

Keywords: friction; slipperiness; bond; electron; phonon; ice; acid; fluid

1 Challenge: Slipperiness of ice

Ice is most slippery of ever known at temperatures even below its melting limit at −22 ℃ under 2,000 atmospheric pressure (200 MPa) pressure. All sorts of surfaces can get slick and slippery if ice and snow abound in winter weather. Slipperiness of snow and ice forms the platform of Winter Olympic Games and many kinds of outdoor entertainments in winter like the jealous skating on ice (see Fig. 1). However, slipperiness of snow and ice has two sides effect. If you are a driver, this is quite troublesome. Ice and snow can make driving inconvenient. Slipperiness of ice is one of the unanswered puzzles since 1859 when Faraday [1] proposed that a quasiliquid kin serves

* Corresponding author: Xi ZHANG, Chang Qing SUN.
E-mail: zh0005xi@szu.edu.cn, Ecqsun@ntu.edu.sg

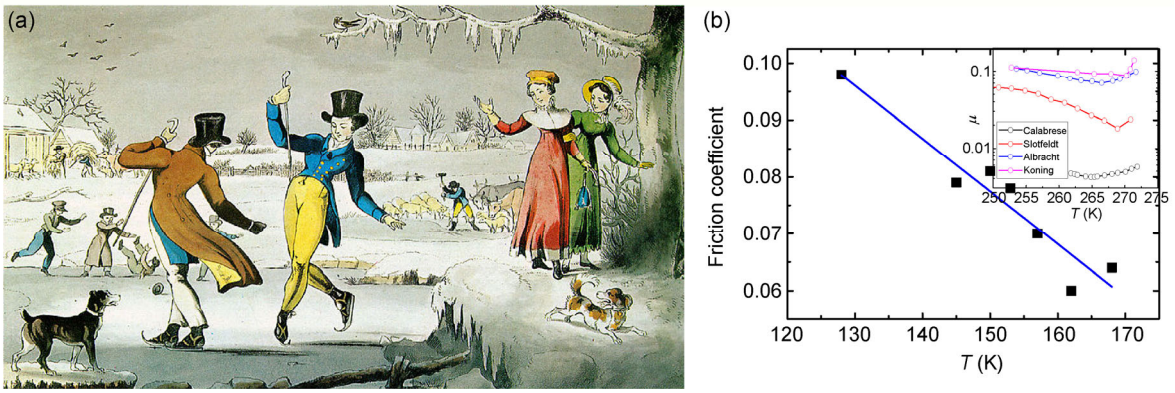

Fig. 1 Is ice covered with a quasiliquid sheet or a supersolid skin [7]? (a) An early 1820's print for the ice-skating scene (Credit: W. Belen, Free Wikipedia). (b) The friction coefficient of steel-pin on ice-disc under 10^{-10} Pa vacuum condition shows linear temperature dependence in the regime of bulk ice (Reproduced with permission from Ref. [8], Copyright Elsevier, 2003). Inset shows friction trends in the quasisolid phase regime (258−273 K) [9] under different conditions [10].

as the lubricant. Debating is still going on with the following possible mechanisms:

(1) Pressure melting creates the quasiliquid lubricant [2, 3].

(2) Friction heating melts ice [4].

(3) Quasiliquid skin forms due to molecular undercoordination [5].

(4) Low-frequency and high-magnitude vibrations associated of surface molecules [6].

2 Clarification: Supersolid lubricant skin

Instead of a quasiliquid layer, friction heating, or pressure melting, ice is covered with a supersolid skin that is elastic, polarized, less dense, and thermally more stable [11−13], as illustrated in Fig. 2:

(1) Molecular undercoordination shortens and stiffens the H–O bond, and meanwhile, lengthens and softens the O:H nonbond with dual polarization of

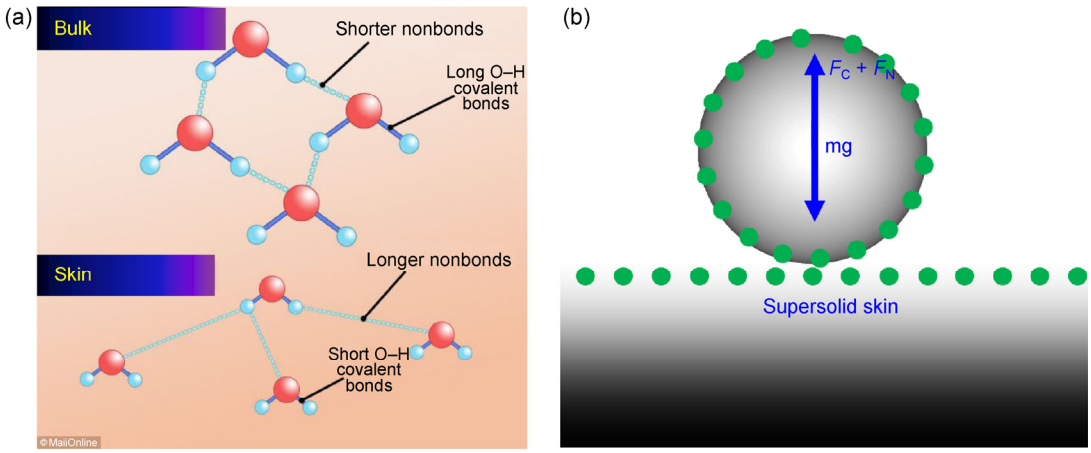

Fig. 2 Elastic Coulomb repulsion makes ice supersolid skin slippery. (a) Undercoordination of H_2O molecules reduces their sizes but enlarges their separations, which softens the O:H nonbond by lowering the frequency and enhancing the amplitude of O:H vibration [12]. (b) The softer O:H springs attached with dipoles not only levitate the object on it but also recover readily from deformation, which make the supersolid skin elastic and slippery. Arrows in (b) denote the force acting on the load: $F_N + F_C - mg = 0$, with F_N, F_C, and mg being the normal force, the Coulomb levitation force, and the weight of the object, respectively. Blue dots represent dipoles associated with O:H soft springs. The skin of any subject is subject to global quantum entrapment and subjective polarization [13], particular at the nanometer scale, which makes the subject nonadditivity [14].

electron lone pairs on oxygen ions (H–O contraction polarizes the lone pair electrons in the first round and that then enhances O–O repulsion in the second).

(2) H–O bond stiffening raises the melting point from 273 to 310 K and the H–O phonon frequency from 3,200 to 3,450 cm^{-1}; O–O elongation lowers the local mass density from 1.0 to 0.75 $g \cdot cm^{-3}$.

(3) The O:H nonbond softening and the O–O dual polarization enhance the viscoelasticity and hydrophobicity of the skin.

(4) Interface Coulomb repulsion between the locally pinned dipoles and the skin elasticity lower the friction at contacts, making ice slippery, which is the same in principle to maglev train and hovercraft (see Fig. 3).

3 History: Wonders of ice friction

3.1 The wonder of ice friction

The first report of sliding on ice comes from Scandinavia Mountains, the source for repeated glaciation that covered much of Eastern, Central, and Western Europe with a particular emphasis on Denmark, Norway, Sweden and Finland, around 7,000 B.C. Rock carvings illustrate the use of a sledge for the transport of heavy goods. The interesting historic record also dates back to 2,400 B.C. when Egyptian carvings employed water lubricant that was poured in front of a sledge to facilitate sliding [10].

In the 15th century [15], Chinese architectures transported large rocks weighing hundreds of tons to the site from 70 km away by using an artificial ice path to build the Forbidden City, an imperial palace, consisting of about a thousand buildings (see Fig. 4), for a typical building. The artificial path was made by pouring water from wells dig aside the path in winter. This kind of ice path overcame limitations of other transport means. For instance, using wooden rollers would require creating a smooth surface on tricky, winding roads. Wheeled carriages would not be able to transport such heavy blocks, even with the technology of the late 1500s.

Understanding the mechanism of friction on ice is particularly important in a broad field of applications, such as motorized vehicle traffic in winter road conditions, glacial movements, and cargo transportation through northern sea ways, design of offshore structures and ice breakers, and ice sports. High friction on ice is desired for motorized vehicle traffic in winter road conditions and the grip of shoe soles on ice to avoid accidents. However, in the field of cargo transportation through northern sea ways and the design of offshore structures, low friction materials are desired to limit maintenance and operation costs, e.g., 70% of the power of an ice breaker ship is consumed to overcome ice friction.

Furthermore, friction and its consequences are of great concern from both a sustainability and quality-of-life point of view, and the economic impact is massive. Indeed, by one estimate, improved attention to tribology (the study of friction, lubrication, and wear) would save developed countries up to 1.6% of their gross national product, or close to $225 billion annually

Fig. 3 Maglev train and hovercraft move frictionlessly because of the interface magnetic repulsion force and the air ejection (Public domain).

Fig. 4 The large stone carving is the heaviest stone in the Forbidden City in Beijing. It weighed more than 300 tons when it was first transported to the site between 1407 and 1420 (Credit: W. Buss and De Agostini).

in the USA alone [16]. Therefore, understanding of ice friction would help in regulating the friction coefficient of solid dry friction and aqueous solute lubrication.

3.1.1 *Factors dominating friction*

In 1785, Coulomb examined five main factors for frictional resistance that involves the nature of materials in contact and their surface coatings, the extent of the contacting surface area, the normal pressure, the length of time that surfaces stay in contact, and the frictional behavior under vacuum as well as under varying ambient conditions namely temperature and humidity [10]. Besides, surface roughness, surface structure, wettability, sliding velocity, and thermal conductivity affect the friction behavior of ice.

3.1.2 *Bi-regime friction coefficient*

Figure 2(b) shows that the friction coefficient of steel-pin on ice-disc in 10^{-10} Pa vacuum depends linearly on temperature in the regime of solid bulk phase [8] but the coefficient (inset) exhibits insignificant temperature dependence in the bulk quasisolid phase regime [9] under different conditions [10]. However, the kinetic friction coefficient between sea ice varies from 0.05 (at −20 ℃) to 0.5 (at −2 ℃) [17]. These temperature trends indicate the intrinsic behavior of ice at different temperature regime or it structure phases.

3.1.3 *Ice on ice: Pressure, temperature, and velosity*

One may expect that the friction coefficient of ice sliding on ice is lower, but observed the opposite. The friction coefficient is sensitive to many factors such as pressure, temperature, and the velocity of sliding. Sukhorukov and Loset [17] examined the effects of sliding velocity (6–05 mm/s), air temperatures (−2 to −20 ℃), normal load (300–2,000 N), presence of sea water in the interface, and ice grain orientation with respect to the sliding direction on the friction coefficient of sea ice on itself. The kinetic friction coefficient of sea ice on sea ice varies from 0.05 (at −20 ℃) to 0.5 (at −2 ℃), regardless of the presence of sea water in the sliding interface. The friction coefficient is independent of the velocity when sliding occurs between natural ice surfaces. As the contacting surfaces became smoother, the kinetic friction coefficient started to depend on the velocity, as predicted by existing ice friction models [10].

Kennedy and coworkers [18] reported that the friction coefficient μ of ice on ice varies with sliding velocity, 0.03 at 5×10^{-2} m/s and 0.58 at 5×10^{-7} m/s within the temperature range from −3 to −40 ℃ under normal pressure of 0.007–1.0 MPa. Generally, μ decreases with increasing velocity and temperature, but it is relatively insensitive to both pressure and grain size. The friction coefficients for freshwater and saltwater ice were almost indistinguishable at higher temperatures (−3 and −10 ℃), but saline ice had lower friction coefficient at lower temperatures with unknown reasons.

Schulson and Fortt [19] measured the friction coefficient of freshwater polycrystalline ice sliding slowly (5×10^{-8} to 1×10^{-3} m/s) upon itself at temperatures from −175 to −10 ℃ under low normal stresses ($\leqslant$ 98 kPa). The coefficient of kinetic friction of smooth surfaces varies from μ_k = 0.15 to 0.76 and, at elevated temperatures ($\geqslant$ −50 ℃), which exhibits both lower velocity strengthening (<10^{-5} to 10^{-4} m/s) and higher velocity weakening of the friction. At intermediate temperatures of −100 and −140 ℃, the kinetic coefficient appears to not exhibit significant dependence upon velocity. However, at the low temperature of −175 ℃, the coefficient of kinetic friction exhibits moderate velocity strengthening at both the lowest and the highest velocities but velocity independence over the range of intermediate velocities.

3.2 Quasiliquid skin notion

Scientists have heavily debated the seemingly simple question of why ice is slippery since 1850 when Faraday [1] firstly proposed that a liquid or a quasiliquid layer serves as the lubricant making ice slippery after his experiment: he pressed two cubes of ice against each other submerged in 0 ℃ water, and they fused together. Faraday argued that the liquid layers remain on a surface but they froze solid when they were at the interface. He also used this mechanism to explain the observation of ice regelation—ice melts under compression and freezes again when the pressure is relieved [20].

Intuition indicates that liquids are mobile whereas solid surfaces are relatively rigid. Asking why ice is slippery is thus roughly equivalent to asking how a liquid or quasiliquid layer can occur on the ice surface in the first place. The presence of liquid reduces friction between solids, that is why water spilled on a kitchen floor or rainwater on asphalt or concrete can create the same kinds of hazards for walkers and drivers that ice can. Therefore, in order to make that solid slippery, a liquid must form on it that allows skates to slip. Therefore, Faraday's proposal of quasiliquid skin was deemed true up to date [11].

How is that thin layer of liquid water going to appear if ice's temperature is well under its melting point? Rosenberg [21], an emeritus professor of chemistry at Lawrence University in Appleton, Wisconsin, featured in ***Physics Today*** 2005 on the history and progress on "why ice is slippery" in terms of pressure melting [2], frictional heating [4], and intrinsic quasiliquid forming or premelting [21].

3.2.1 *Pressure melting*

The conventional explanation, pressure melting, was suggested by James Thomson [2] in 1850 and lately experimentally approved by his brother, William Thomson, Later Lord Kevin [3], in 1850 as a consequence of the higher density of liquid water relative to ice. James Thomason calculated that a pressure of 46.6 MPa would lower the melting point by −3.5 ℃. Kelvin verified that result experimentally. However, James Thomson was not able to explain how hockey players and skaters in Fig. 5 were able to slide at temperatures below −35 ℃ at which temperature and below no pressure melting takes place. Skating is possible at very cold from around −30 ℃, so how is it possible for skaters to skate at this very cold temperature? The player's own weight would not be able to pressure the ice enough to drop the melting temperature of ice and create a thin layer of liquid water. The pressure-melting explanation also fails to explain why someone wearing flat-bottom shoes, with a much greater surface area that exerts even less pressure on ice can also slip on the ice.

The optimum temperature for figure skating is −5.5 ℃ and for hockey is −9 ℃; figure skaters prefer slower, softer ice for their landings, whereas hockey players exploit the harder, faster ice. Indeed, skating is possible in climates as cold as −30 ℃ and skiing waxes are commercially available for such low temperatures. In his 1910 account of his last expedition to

Fig. 5 Ice skating provides insufficient pressure to melt ice but lowers the melting point by only 0.24 ℃ (Galina Barskaya/Dreamstime.com). With negligible friction or compression, a penguin can hardly stand still on ice (BBC online).

the South Pole, Robert Falcon Scott [21] tells of skiing easily at −30 ˚C though the snow surface is sand-like at −46 ˚C. But surprisingly, even with little evidence in its favor, pressure melting was dominant for more than a century and still remains as the dominant explanation of the slipperiness of ice in many text books.

Ice skating is given as an example of regelation to create liquid to lubricate ice; however the pressure required is much greater than the weight of a skater. Additionally, regelation does not explain how one can ice skate at temperatures below the limit of −22 ˚C. If the contacting area of the skate to ice is 150×10^{-6} m^2 (1 mm wide and 150 mm long) and the skater weighs 500 N, the pressure applied will be 3.3 MPa. As the melting point of ice falls by 0.0072 ˚C for each additional atm (0.1 MPa) of pressure applied, the melting point will drop by 0.24 ˚C only. Therefore, skating provides insufficient pressure for melting ice (Fig. 5).

3.2.2 *Friction heating*

Bowden and Hughes [4] proposed in 1939 the frictional heating as an alternative mechanism. Friction is the force that generates heat whenever two objects slide against each other. If you rub your hands together, you can warm them up. When a skate moves on the surface of ice, the friction between the skate and the ice generates heat that melts the outermost layer of ice. Bowden and Hughes did an experiment at a research station in Switzerland to maintain temperatures below −3 ˚C using solid CO_2 and liquid air. Using surfaces of wood and metal, they measured the effects of static and kinetic friction on ice melting. They concluded that frictional heating was responsible for melting ice. Although frictional heating may answer why ice is slippery when moving, this theory does not explain why ice can be so slippery even for someone, such as a penguin, standing still on it.

3.3 Quasiliquid skin formation

3.3.1 *Surface premelting*

Faraday [1] suggested that a film of water on ice would remain liquid on the surface of a single piece but the water layer would freeze when placed between two pieces of ice. However, he was not able to reason why the liquid layer forms at the molecular level with neither pressure melting nor friction heating.

In 1949, Gurney [5] suggested that an intrinsic liquid film forms on ice. Gurney hypothesized that molecules, inherently unstable at the surface due to the lack of molecules above them, migrate into the solid until the surface becomes stable, which prompts the formation of a liquid phase. If appreciable atomic migration takes place, the surface of a crystalline solid melts, like surface melting point depression happened to most normal substance [22], and the solid is covered with a thin liquid film under a tension force greater than that of the corresponding supercooled liquid. This tension force is numerically equal to the free energy of the surface. If such a solid is subsequently cooled to a temperature at which atomic migration effectively ceases, it will have frozen its surface with a tension force corresponding to thermal equilibrium at some higher temperatures.

3.3.2 *Interface phonons and electrons*

At the atomic scale, Krim [6, 16] proposed that interface atomic lattice vibration and the electronic charge play significant roles in friction. When atoms close one surface are set into motion, atoms in both surfaces create waves in terms of phonons. The amount of mechanical energy transformed into phonons depends on the sliding substances. Solids are much like musical instruments in that they can vibrate only at certain distinct frequencies, so the amount of mechanical energy consumed will depend on the frequencies actually excited. If the "plucking" action of the atoms in the opposite surface resonates with one of the frequencies of the other, then friction arises. It is not resonant with any of the other surface's own frequencies, and then sound waves are effectively generated.

On the other hand, the smaller the resulting amplitude of vibration, the greater the friction will be from the "rubbing" action of the film sliding about on the substrate. For insulating surfaces, friction arises from the attraction of unlike charges attached to the surfaces, like a balloon being rubbed on hair and left to cling to a wall. In 1989, Krim and coworkers [6] found the friction coefficient of Krypton films on

crystalline gold surfaces is lower when dry; adding a liquid film raises the coefficient by five times, instead. Applying electric field cross the contacting interface can also affect the coefficient of friction [23].

3.3.3 *Diffraction examination of premelting*

Since 1960s, a variety of experimental approaches, performed under various conditions, has been brought to bear on the premelting problem to determine the temperature range and thickness of the postulated quasiliquid layer. In 1969, Orem and Adamson [24] found that impurity adsorption promotes surface melting. Physical adsorption of simple hydrocarbon vapors on ice creates a liquid-like layer on the surface of ice. The adsorption of *n*-hexane on the surface of ice can form liquid-like layer at temperatures above −35 ℃. These researchers interpreted their results as indicating the onset of ice's surface premelting at −35 ℃. In the 1990s, chemistry Nobel laureate Mario Molina and coworkers [25] attributed the adsorption of hydrochloric acid on polar stratospheric clouds to the existence of a liquid-like layer on ice, which plays a role in the destruction of ozone.

Nuclear magnetic resonance (NMR) [26] spectroscopy suggested liquid layer formation on ice: below the melting point there is a narrow absorption line, not the broad line one would expect from a periodic solid. Molecules at the surface between 20 and 0 ℃ rotate at a frequency five orders of magnitude greater than those in bulk ice, and about 1/25 as fast as those in liquid water. The self-diffusion coefficient of molecules is two orders of magnitude larger than that in bulk ice. Using proton backscattering, Golecki and Jaccard [27] found in 1977 that surface vibrations of the oxygen atoms are roughly 3.3 times the amplitude of their bulk value, and estimated an amorphous layer 10 times thicker than what NMR measurements had estimated. But, unlike NMR, the proton backscattering measurements were made under high vacuum, a condition markedly different from the finite vapor pressures at which surface melting typically occur. Molecules perform differently under the ambient vapor pressure.

X-ray diffraction (XRD) study [28] conducted in 1987 suggested that the intermolecular distance on the ice surface is shorter than that of ice's bulk interior and slightly shorter than that in liquid water. In the mid-1990s, Dosch and coworkers [29] found a liquid−like layer on the different crystallographic ice surfaces between −13.5 and 0 ℃. The surface layer exhibits rotational disorder with intact long-range positional order well below the surface melting temperature. At the surface-melting temperature, a completely disordered layer exists on the surface above the rotationally disordered layer.

Low-energy electron diffraction (LEED) experiments conducted in 1996 by Li and Somorjai [30] also suggested the presence of quasiliquid layer when they probed the surface of thin layers of ice. LEED is a technique that uses electrons to determine the surface structure of a crystal in the same way as XRD reveals the crystal structure of a solid. By observing how electrons bounced off ice surface, they suggested that the rapidly vibrating oxygen ions (H–O bond) actually make the surface of ice slippery. These "liquid-like" water molecules do not move from side to side—only up and down. If the atoms moved from side to side, the layer would actually become liquid, which is what happens when the temperature rises above 0 ℃.

3.3.4 *AFM sliding and scratching friction*

In 1998, Döppenschmidt and Butt [31] using an atomic force microscopy (AFM), measured the thickness of the liquid-like layer on ice, in temperatures above −35 ℃. As illustrated in Fig. 6, capillary contacting forces on the liquid surface prompted the cantilever tip of the AFM to jump into contact with the solid ice once it reached the much softer layer's level. The upper limit in thickness of the liquid-like layer varied from 70 nm at −0.7 ℃, 32 nm surface melting starts at −1 ℃, to 11 nm at −10 ℃. Their results indicated that surface melting starts at about −33 ℃. The temperature dependence of the thickness follows roughly a rule, $d \propto -\log\Delta T$, where ΔT is the difference between the melting temperature and the temperature of detection.

The addition of salt could increases the thickness of the liquid-like layer. However, dragging the AFM tip across the surface of ice derived high friction of ice, which indicates that while the top layer of ice may be liquid, it is too thin to contribute much to slipperiness except near the melting temperature.

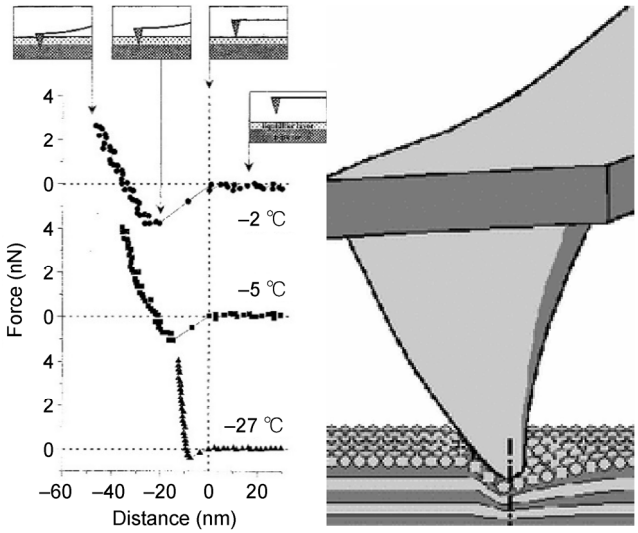

Fig. 6 Atomistic scratching (plastic dislocation) and sliding (elastic deformation) friction. Approaching part of force curves measured at different temperatures. "Zero distance" was defined at the surface of the liquid-like layer. The assumed position of the tip is indicated schematically for the force curve taken at −2 ℃ (Reproduced with permission from Ref. [31], Copyright ACS Publications, 2000).

3.3.5 X-ray reflection

However, Engemann and coworkers [32] examined in 2004 the x-ray reflectivity at the interface between ice and solid silicon dioxide and calculated the thickness and density of the liquid layer at temperatures between −25 and 0 ℃, as illustrated in Fig. 7. They derived that the skin is a "high-density form of amorphous ice"—the density of the quasiliquid skin varied from that of liquid water at its melting point to 1.16 g/cm^3 at −17 ℃. The thickness of the quasiliquid layer follows the relationship:

$$L(T) = (0.84 \pm 0.02)\mathrm{Ln}\frac{17 \pm 3}{T_\mathrm{m} - T}(\mathrm{nm})\,.$$

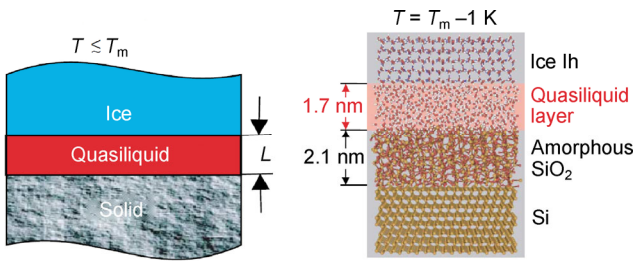

Fig. 7 High-density quasiliquid skin forms between ice and amorphous SiO_2 at $T \geqslant T_\mathrm{m} - 17$ K and its thickness increases with temperature (Reproduced with permission from Ref. [32], Copyright AIP Publishing, 2004).

This experiment supports quasiliquid skin mechanism as the main cause of ice's slipperiness observed at −17 ℃ and above.

3.4 A common supersolid skin covers both water and ice

From the perspective of O:H–O bond cooperative relaxation between undercoordinated water molecules, Sun and coworkers [33] proposed and verified the skin supersolidity [11, 12] in 2013 using quantum calculations and electron and phonon spectrometrics. Molecular undercoordination not only disperses the quasisolid phase boundaries but also results in a temperature independent supersolid skin. Instead of the high-density quasiliquid skin, the elastic, less dense, polarized supersolid phase presents due to molecular undercoordination at the skins of water and ice. An elastic Coulomb-levitation mechanism is responsible not only for ice slipperiness and water hydrophobicity but also for low friction of dry solid such as graphite, nitrides, oxides, and fluorides because of the presence of nonbonding electrons [33].

4 Quantitative resolution

4.1 Skin O:H–O bond relaxation

The O:H–O bond contains both the O:H nonbond and the H–O bond rather than either of them alone. Segmentation of the O:H–O bond is necessary into a shorter and stiffer H–O covalent bond with a stronger exchange interaction and a longer and softer O:H nonbond with a weaker nonbond (vdW-like) interaction, as illusrated in Fig. 8 [12, 34]. The vdW-like interaction contains electrostatic interaction between the lone-pair and the H^+ proton, so the nonbond interaction is slightly stronger than the ideal vdW bond that denotes purely dipole–dipole interaction. The H^+ proton always remains closer to the O (right-hand side of Fig. 8) without any frustration and keeps away from the other O atom because of the much stronger H–O exchange interaction than the weaker O:H nonbond. The O:H–O bond links the O–O in both the solid and liquid H_2O phase, regardless of phase structures [35].

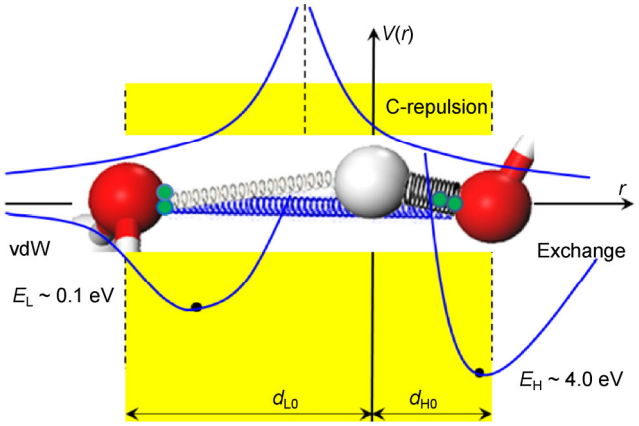

Fig. 8 Asymmetrical, short-range interactions for the segmented O:H−O bond include the O:H van der Waals (vdW)-like nonbond interaction (left-hand side), the H−O bond exchange (right-hand side) interaction, and the Coulomb repulsion between electron pairs on adjacent O^{2-} ions. One switches off a particular potential and the other at the boundary, or at the atomic site, when it moves across the boundary (Reproduced with permission from Ref. [36], Copyright Elsevier, 2015).

Generally, bond order loss shortens and stiffens the bond between undercoordinated atoms by up to 12% for a flat skin of an fcc geometry, which enhances the bond energy by 45% and depresses the atomic cohesive energy by 62% for a metal such as gold and copper [37]. The enhanced bond energy raises the skin elasticity by 67% and lowers the local meting temperature by 63% [13]. However, for water and ice, molecular undercoordination shortens the H–O bond and stiffens its phonon. The O:H nonbond responds to undercoordination oppositely in length and phonon frequencies because of its weak interaction and the O–O repulsion. No electron exchange exists in the O:H nonbond as observed using AFM [38].

Figure 9 features the residual length spectra (RLS) for the MD-derived d_x of ice [11]. Subtracting the length spectrum calculated using the 360-molecular unit cell without skin from that with a skin resulted in the RLS. Features above the lateral x-axis represent the length gain and features below the axis represent the length loss due to the presence of the skin. The RLS shows that d_H contracts from the bulk value of about 1.00 to about 0.95 Å at the skin, while d_L elongates from the bulk value of 1.68 to 1.90 Å with high fluctuation as a broad peak. This cooperative relaxation lengthens the O–O by 6.8% (=1 − (0.95 + 1.90)/(1.0 + 1.68)) or lowers the mass density to 82% from the bulk standard on the base of $\rho \propto d_{O-O}^{-3}$. d_H = 0.93 Å peak even corresponds to the undercoordinated H–O radicals, whose vibration frequency is around 3,650 cm^{-1} [12]. The standard length is d_H = 1.0004 and d_L = 1.7946 Å at 4 ℃ [35].

According to the density–geometry–length correlation of molecules packed in water and ice [35], the measured d_{O-O} of 2.965 Å for liquid water skin [39] gives rise to d_H = 0.8406 Å and d_L = 2.1126 Å, which correspond to a 0.75 g/cm^3 skin mass density [11]. In comparison, the MD derived from Fig. 9 a density of 0.82 g/cm^3. These values, 0.75–0.82 g/cm^3, are much lower than 0.92 g/cm^3 for bulk ice or bulk water at 4 ℃, which is much lower than the 1.16 g·cm^{-3} for amorphous quasiliquid skin, derived from X-ray reflection [32].

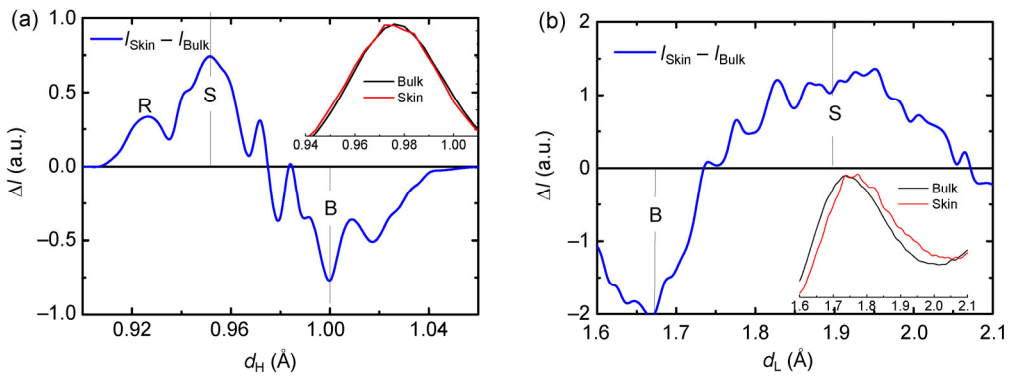

Fig. 9 MD-derived RLS reveals that (a) d_H contracts from the bulk value (B) 1.00 to 0.95 Å for the skin (S) and to 0.93 Å for the H−O free radicals (R), which is coupled with (b) d_L elongation from the bulk value (B) of 1.68 to 1.90 Å, with high fluctuation. Insets show the raw length spectra of the unit cell with (denoted "skin") and without skin presence (denoted "bulk") (Reproduced with permission from Ref. [11], Copyright RSC Publications, 2014.)

4.2 Identical ω_H for skins of water and ice

Figure 10 shows the residual phonon spectra (RPS) in comparison to the measured ω_H RPS for both water and ice given in Fig. 11 [40]. The valleys of the RPS represent the bulk feature, while peaks feature the skin attributes. A proper offset of the calculated RPS is necessary, as the MD code overestimates the intra- and intermolecular interactions [9]. As expected, the ω_L undergoes a redshift, while the ω_H undergoes a blueshift with multiple components. The ω_H blueshift results from the stiffening of the skin H–O bonds (S) and the free H–O radicals (R). The ω_L redshift arises from O–O repulsion and polarization. The polarization in turn screens and splits the intramolecular potential, which adds another ω_H peak (denoted P as polarization) with a frequency being lower than that of the bulk valley (B), which was ever regarded as a second type of the O:H nonbond.

Most strikingly, the measured RPS in Fig. 11 shows that the skins of water and ice share the same ω_H value of 3,450 cm^{-1}, which indicates that the H–O bond in both skins is identical in length and energy, according to the relationship $\omega_H \propto (E_H/d_H^2)^{1/2}$. The kin ω_L of ice may deviate from that of liquid water because of the extent of polarization, which is subject to experimental verification. Nevertheless, the skin ω_H stiffening agrees with the DFT–MD derivatives that the ω_H shifts from ≈ 3,250 cm^{-1} at 7 Å depth to ≈ 3,500 cm^{-1} of the 2 Å skin of liquid water [41]. Therefore, it is neither the case that an ice skin forms on water nor the case that a liquid skin covers ice. Rather, an identical supersolid skin covers both. In the supersolid skin, molecules shrink their size and enlarge separations, the O:H vibration frequency becomes lower, and the amplitude is expected greater, which promotes the slipperiness of ice against other objects.

The skins of water and ice share the same ω_H of 3,450 cm^{-1}. The peak intensity changes with the scattering from ice and water.

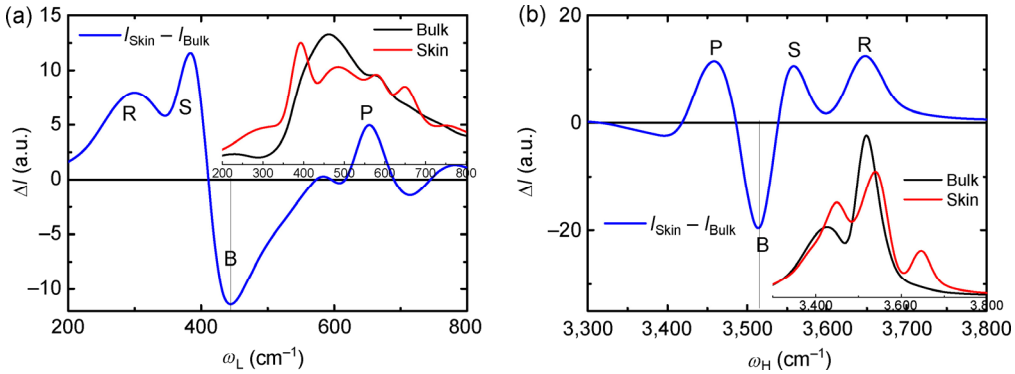

Fig. 10 MD-derived RPS for the (a) ω_L and (b) ω_H of 200 K ice [11]. Insets in (a) and (b) show the raw spectra of calculations. Features S corresponds to the skin H–O bond; R corresponds to the free H–O radicals; the P component arises from the screening and splitting of the crystal potential by the polarized nonbonding electrons.

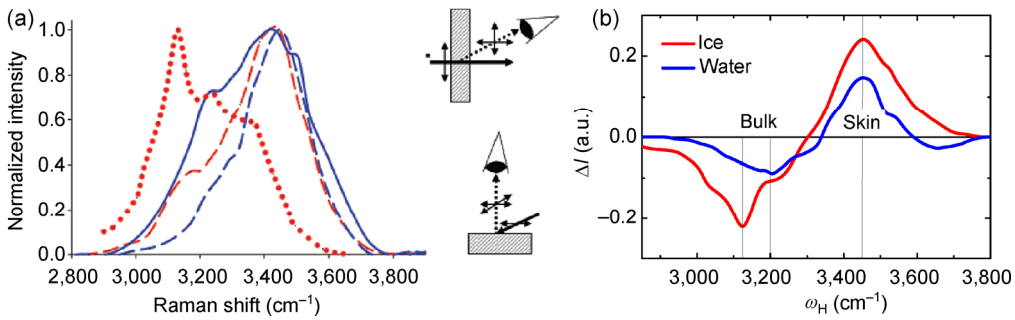

Fig. 11 (a) Raman ω_H spectroscopy of water (in blue, at 25 ˚C) and ice (red, at −20 and −15 ˚C) [40] collected at 87° (peaks toward higher frequency) and 0° with respect to the surface normal and water (side views). (b) The experimental RPS of water and ice distills the skin peak from the bulk as valley contribution to the spectra [11].

4.3 Skin electron entrapment versus H–O bond energy

Table 1 features the DFT-derived Mulliken charge accumulation at the skin and in the bulk of water. O increases its net charge from the bulk value from −0.616 to −0.652 e when located at the skin. The net charge of a water molecule increases from 0.022 to −0.024 e correspondingly, which confirms the first round polarization of the electron lone pair by the entrapped O 1s core electrons due to H–O bond contraction [11].

The following formulates the skin H–O bond energy E_H(Skin) and the atomic O 1s energy $E_{1s}(0)$. Table 1 lists the derivatives [22]:

$$\frac{\Delta E_{1s}(N)}{\Delta E_{1s}(\infty)}=\frac{E_{1s}(N)-E_{1s}(0)}{E_{1s}(\infty)-E_{1s}(0)}=\frac{E_H(N)}{E_H(\infty)}=\frac{T_C(N)}{T_C(\infty)}=\left(\frac{d_H}{d_{H0}}\right)^{-m} \quad (1)$$

The E_H(Skin) = 3.97 × (538.1/536.6) = 4.52 eV is compatible with the value of 4.66 eV for breaking the H–O bond of H_2O molecules deposited on a TiO_2 surface in less than a monolayer coverage using laser excitation [45]. The deviation ΔE_H(Skin) = 0.14 eV (about 3%) arises mainly from molecular undercoordination in these two situations—one is the water skin and the other is the even less coordinated water molecules deposited on TiO_2 surface, which indicates that interaction between water molecules and the hydrophobic TiO_2 surface is very weak because the presence of an 5~10 Å thick air gap in the hydrophobic contacts [46].

With the known values of $(d_H, E_H)_{Skin}$ = (0.84 Å, 4.52 eV) and $(d_H, E_H)_{Bulk}$ = (1.0 Å, 3.97 eV) and the $E_H(1)$ = 5.10 eV, the bond nature index is estimated as m = 0.744 and the $d_H(1)$ = 0.714 Å of a monomer. The densely and locally entrapped core electrons of the undercoordinated water molecules polarize in a dual-process the nonbonding electrons.

Following the same trend as "normal" materials, molecular undercoordination imparts to water local charge densification [47–52], binding energy entrapment [48, 53–55], and nonbonding electron polarization [50]. For instance, the O 1s level shifts more deeply from the bulk value of 536.6 eV to 538.1 eV and 539.7 eV when bulk water is transformed into skin or into gaseous molecules [42, 43]. However, an ultrafast liquid-jet UPS [50] resolved the vertical bound energies (being equivalent to work function) of 1.6 eV and 3.3 eV for the solvated electrons in the skin and in the bulk center of the solution, respectively. In addition, the bound energy decreases with the number n of the $(H_2O)_n$ clusters, evidence that undercoordination substantially enhances nonbonding electron polarization [12].

Table 1 DFT-derived charge localization at the skin and in the bulk of ice and derivatives (in bold) based on the referenced data using Eq. (1). Negative sign represents net electron gain.

	Skin	Bulk	$(H_2O)_1$	O atom
q_O	–0.652	–0.616	—	—
q_H	0.314	0.319	—	—
Net q of H_2O	–0.024	0.022	—	—
E_{1s} (eV) [42–44]	538.1	536.6	539.7	525.71
E_H (eV)	4.52/4.66	3.97 [35]	5.10 [45]	—
T_m (K)	311/320	273	—	—

4.4 Skin thermal stability

Generally, atomic undercoordination depresses the critical temperature for phase transition of many substances because of the undercoordination reduced atomic cohesive energy, $T_C \propto zE_z$, where z is the atomic coordination number and E_z is the cohesive energy per bond. The phase transition includes liquid–solid, liquid–vapor, ferromagnetic, ferroelectric, and superconductive transitions [13]. The skin melting temperature $T_{m,s}$ drops or rises depending the nature of the chemical bond, $T_{m,s}/T_{m,b} = z_s/z_bC_z^{-m}$, where m is the bond nature index and $C_z = 2[1+\exp[(z-12)/(8z)]]^{-1}$ is the contraction coefficient of bond between undercoordinated atoms. According to the BOLS notion, the skin $T_{m,s}$ is 40% and 62% of the bulk metal (m = 1) and silicon (m = 4.88) as the effective atomic CN of the top layer is 4 and the bulk is 12 for an fcc structure standard [22].

However, for water molecules, the T_C is proportional to either E_H or the E_L only, depending on the nature of phase change, because of the "isolation" of the H_2O molecule by its surrounding lone pairs. For instance, E_L determines the T_C for evaporation T_V, as this process dissociates the O:H nonbond. The E_L also determines the freezing temperature as defined by the specific heat disparity [56]. The E_H dictates T_m(Skin)

that is estimated from the correlation between the T_C(N) and the ΔE_{1s}(N) from Eq. (1):

$$\frac{T_C(\text{Skin})}{T_C(\infty)} = \frac{T_m(\text{Skin})}{273} = \frac{E_H(\text{Skin})}{E_H(\text{Bulk})} = \frac{4.59 \pm 0.07}{3.97},$$

which yields the skin melting temperatures in the range of 315 ± 5 K. It is therefore not surprising that water skin performs like ice or gel at room temperature and that the monolayer water melts at about 325 K [57].

4.5 Skin viscoelasticity

The polarization of molecules enhances the skin repulsivity and viscoelasticity. The high viscoelasticity and the high density of skin dipoles are essential to the superhydrophobicity and superlubricity at contacts [58]. According to the BOLS–NEP notion [13], the local energy densification stiffens the skin and the densely and deeply entrapped bonding charges polarize nonbonding electrons in dual process to form anchored skin dipoles [33]. The negative charge gain and the nonbonding electron polarization provide electrostatic repulsive forces lubricating ice.

Table 2 features the MD-derived thickness-dependent γ, η_s, and η_v of ice films. Reducing the number of molecular layers increases them all. The O:H–O cooperative relaxation and associated electron entrapment and polarization enhances the surface stress to reach the value of 73.6 mN/m for five layers, which approaches the measured value of 72 mN/m for water skin at 25 ˚C. Generally, the viscosity of water reaches its maximum at temperatures around T_m [59].

4.6 Skin repulsivity and hydrophobicity

Measurements, shown in Fig. 12, verified the presence of the repulsive forces between a hydrated mica substrate and the tungsten tip contacts at 24 ˚C in AFM measurements [60]. Such repulsive interactions appear at 20%–45% relative humidity (RH). The repulsion corresponds to an elastic modulus of 6.7 GPa. Monolayer ice also forms on a graphite surface at 25% RH and 25 ˚C [61]. These observations and the present numerical derivatives evidence the presence of the supersolidity with repulsive forces because of bonding charge densification, surface polarization, and T_m elevation due to undercoordination induced O:H–O bond cooperative relaxation.

Table 2 Thickness-dependent surface tension γ and viscosity η.

Number of layers	15	8	5
γ (mN/m)	31.5	55.2	73.6
η_s (10^{-2} mN·s/m^2)	0.007	0.012	0.019
η_v (10^{-2} mN·s/m^2)	0.027	0.029	0.032

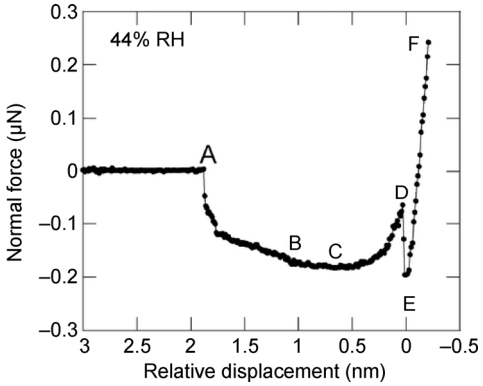

Fig. 12 Normal force profiles between mica and tungsten tip at 44% RH. Point A is the initiation of water nucleation and condensation; B and C are the formation of a complete water bridge cross the tip and substrate; D is the maximum attractive force before the tip–substrate contact; E denotes the sudden drop of force; and F indicates the tip–substrate contact repulsive force (Reproduced with permission from Ref. [60], Copyright ACS Publications, 2009).

4.7 Elastic electro-levitation mechanism

It is convenient to adapt the concept of supersolidity from the superfluidity of solid ^{4}He at mK temperatures. The skins of ^{4}He fragments are highly elastic and frictionless with repulsion between them when set in motion [33]. It is clarified in 2012 that the "supersolidity" arises from the shear elasticity of the ^{4}He fragment [62–64]. But the interface repulsivity between fragments is essential to ensure the frictionless motion of the fragment. The skins of water and ice form an extraordinary "supersolid" phase [11] that is elastic [40], hydrophobic [65, 66], polarized [50, 67], less dense [39], and thermally stable [57], because of the densely entrapped bonding electrons [42–44, 53] and the dual polarization. The fewer the molecular neighbors there are, the smaller the water molecule size and the greater the molecular separation is, and therefore, the greater extent the repulsivity and supersolidity will be.

4.7.1 *O:H phonon vibration amplitude and frequency*

According to the BOLS–NEP notion [36], molecular undercoordination shortens and stiffens the intramolecular H–O bond and meanwhile, lengthens and softens the intermolecular O:H–O bond because of the Coulomb repulsion between electron pairs on adjacent oxygen ions. The H–O will vibrate faster and the (H_2O):(H_2O) oscillate slower at the skin. The dual polarization increases the local charge of O ions at the skin.

MD (Figs. 9 and 10) and DFT (Table 1) calculations confirmed so. The O:H nonbond contracts from the bulk value of 1.0 to 0.95 Å for the skin and 0.93 for H–O radical and the H–O expands from 1.65 to 1.90 Å. The O:H phonon frequency shifts from the bulk value of 450 to 400 for the skin and to 300 cm^{-1} for those close to free H–O radicals. The H–O phonon shifts from 3,500 to 3,550 and 3,650 cm^{-1} for the skin and H–O radicals, disregarding the artifact of the potential splitting and polarization effect.

The curvature of an interatomic potential generally approximately conserves [13], which correlates the amplitude and frequency of an oscillator at vibration:

$$\mu(\omega x)^2 = \left(\frac{\partial^2 u(r)}{\partial r^2}\bigg|_{r=d}\right)x^2 = \text{const.}$$

The O:H–O bond segmental vibration amplitudes at the skin or associated with a radical vary from that of the bulk as,

$$\frac{x_{\text{skin}}}{x_{\text{bulk}}} = \frac{\omega_{\text{bulk}}}{\omega_{\text{skin}}} \cong \begin{cases} 200/100 = 2 & (\text{skin O:H}) \\ 3200/3450 = 64/69 & (\text{skin H-O}) \end{cases}.$$

Therefore, in addition to the stronger dual polarization, the greater amplitudes and the lower frequencies of the skin O:H oscillators are responsible for the slipperiness of ice, as illustrated in Fig. 2(b). The soft springs deform easily when they are compressed and then recover their original states once the sliding compression is relieved. If the compression force is too large, the O:H nonbond breaks, the friction coefficient increases sharply—scratching other than sliding.

4.7.2 *High friction coefficient of ice on ice*

As shown in Fig. 1(b), the kinetic friction coefficient of steel on ice ranges from 0.01 to 0.1. The friction coefficient of ice on ice varies unexpectedly from 0.03 at 0.05 m/s and 0.58 at 5×10^{-7} m/s sliding velocity, within the temperature range of −3 and −40 ˚C under normal pressure of 0.007–1.0 MPa [18]. The following rules govern the unexpected high friction coefficient for ice on ice:

(1) Regelation takes place when two pieces of ice contact at temperatures above −22 ˚C. As observed by Faraday [1], 0 ˚C water can fuse two pieces of ice under a slight compression.

(2) Coordination recovers as water molecules tend to recover their unoccupied neighbors, reserving energetically favorable sp^3 bonding configurations of oxygen [68, 69].

(3) O:H phonon resonant coupling occurs when two pieces of ice are brought contact, as noted by Krim [6]. Higher vibration amplitude and identically lower frequency O:H oscillators hinder their sliding motion.

(4) However, the friction coefficient for saline ice on normal ice is expected lower because the solute ionic electrification shifts the O:H phonon frequency from ~200 to ~100 cm^{-1}, which decouples the interface phonon resonant.

4.7.3 *Two-regime friction: phonon criterion*

Figure 13 illustrates the O:H–O bond relaxation dynamics in the solid and in the quasisolid phases of bulk water, which discriminates why the friction coefficient shows two temperature regimes.

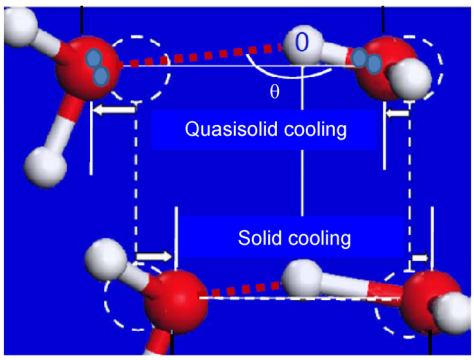

Fig. 13 O:H–O bond relaxation in the solid (T < 258 K) and in the quasisolid (258 ⩽ T ⩽ 277 K) phases of bulk because of the segmental specific disparity [9]. O:H nonbond elongation and its vibration amplitude elevation lowers the friction coefficient in the quasisolid phase as ice cools (Reproduced with permission from Ref. [36], Copyright Elsevier, 2015.)

In the quasisolid phase of 258–273 K range, the relative specific heat $\eta_H/\eta_L < 1$, the H–O bond contracts at cooling, which lengthens the O:H nonbond and softens its phonons with higher vibrating amplitude, which enhances the slipperiness of ice as it cools though measurement varies from situation to situation.

In the solid phase below 258 K, the O:H nonbond contracts at cooling because of $\eta_H/\eta_L > 1$. Cooling contraction results in its higher frequency and smaller magnitude of vibration. The O:H nonbond contraction and its vibration amplitude reduction increase the friction coefficient of ice. This trend carries on as it cools so the friction coefficient increases when temperature is lowered, as shown in Fig. 1(b).

4.7.4 AFM friction: scraching or sliding?

Generally, one talks about friction of an object sliding on ice, which gives a lower friction coefficient because of the elastic atomic deformation. However, as shown in Fig. 6, an AFM in contacting mode derived high kinetic friction coefficient of 0.6 in the temperature range of –20 and –40 ˚C, which is compatible to the static coefficient measured in macroscopic experiments [70]. The AFM tip scratching into the skin of several nanometers thick breaks the skin O:H nonbond with resistance of the high viscosity during scratching. The tip does not entertain the superlubricating skin for sliding but experienced the creep and viscosity resistance because of the plastic dislocation. Therefore, care needs to be taken when one measures the atomistic friction coefficient using an AFM.

5 Solid dry friction

5.1 Supersolidity of ^{4}He crystals: Elasticity and repulsivity

Helium is the noblest amongst all elements: the interaction between even its own atoms is so weak that it solidifies only under intense pressure and extremely low temperatures. If the pressure is reduced to 2.5 MPa at the absolute zero temperature, quantum-mechanical fluctuations of the atoms' positions become so large that the solid melts, becoming a "quantum liquid". No crystalline solid is perfect—there are always some vacancies in the crystal lattice where atoms are missing—and in 1969, Andreev and Lifshits [71] proposed that helium's large quantum fluctuations might, at zero temperature, stabilize a dilute gas of vacancies within the solid. Atoms of the prevalent isotope ^{4}He are bosons (they have zero spin), and so vacancies in solid ^{4}He can also be thought of as bosons. The vacancies can thus condense to form an exotic phase known as a Bose–Einstein condensate that suffuses the solid. This "supersolid" phase, lately referred to shear elasticity, would share some commensurateness with a superfluid—namely, frictionless flow—but at the same time have a non-zero shear modulus, a defining characteristic of a solid. Figure 14 illustrates the supersolid state of solid ^{4}He. Only 1% undercoordinated ^{4}He atoms present at boundaries of the fragments make the fragments frictionless at torsional motion.

Supersolidity describes the coexistence of solid and superfluid properties in a quantum crystal. The phenomenon was discovered in 2004 by Kim and Chan [62, 73] when they measured the resonance period of a small cylindrical box oscillating around a torsion rod. The box contained solid ^{4}He at temperature below 100 mK, and the oscillation frequency increases as if 1% of the helium mass had ceased moving with the box. To run the ^{4}He supersolidity experiment, they hang the disk from a stiff rod and oscillate the disk back and forth. By measuring the frequency of oscillation, they detected whether the solid ^{4}He behaves like a supersolid—high shear elasticity and repulsivity in the contact normal. An oscillating disk of normal matter, for example, behaves as expected: because the atoms are rigidly linked, they rotate together. In an oscillating disk of supersolid

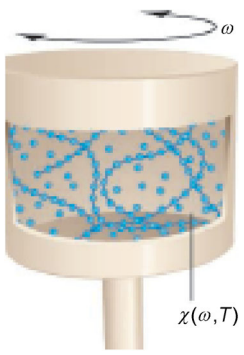

Fig. 14 Supersolidity of ^{4}He at 2 K temperatures or below [72]. The torsional oscillator is a disk filled with solid ^{4}He of multiple fragments, as denoted with color lines.

matter, many of the atoms rotate, but some do not. Instead, those atoms slip through the lattice like a superfluid, without friction whatsoever, and sit motionless. That reduces the mass of the disk, which allows it to oscillate faster. In fact, the fraction of ^{4}He atoms that refuse to rotate is closer to only 1%.

The same method had been widely used for the detection of superfluidity in a liquid in the absence of viscosity, and the liquid in the box remains at rest while the box walls move. At temperature below 200 mK, ^{4}He crystal is readily decoupled into fragments in a torsional oscillator to exhibit superfluidic nature—frictionless motion without viscosity [62–64]; meanwhile, the ^{4}He crystal fragments are stiffer than expected and hence react elastically to a shear stress applied [74]. The individual ^{4}He segment would be thus both superelastic and superfluidic in motion—the supersolidity meant.

The "supersolid" form of ^{4}He is stiffer, more elastic and frictionless than the normal solid [75]. The superfluidity of ^{4}He solid is usually described in terms of Bose–Einstein condensation or quantum statistics in energy space. All particles occupy the lowest energy states simultaneously. A scenario in real space is infancy though the crystal defects have been recognized as the key to the supersolidity [76]. The superfluidity of ^{4}He solid is related to the quantum defects such as atomic vacancies of 1 nm size or around [77] and the supersolidity is related to structural disorder [78] such as dislocations, grain boundaries, or ill-crystallized regions where the undercoordinated atoms become dominant. According to Pollet et al. [77], inside a dislocation or a grain boundary, the local stress is anisotropic, which is sufficient to bring the vacancy energy to zero, so that the defect is invaded by vacancies that are mobile and superfluidic. Solid ^{4}He could contain a network of defects and if these defects are connected to each other, mass could flow from one side of the crystal to the other without friction. On the other hand, the disorder-induced stiffening could be the result of dislocations becoming pinned by isotopic impurities (i.e., ^{3}He atoms even at very small concentrations).

Later ultrasound and torsional oscillator studies [79, 80], however, evidence that shear modulus stiffening is responsible for at least a fraction of the period drop found in bulk solid helium samples. The experimental configuration of Kim and Chan makes it unavoidable to have a small amount of bulk solid inside the torsion cell containing the Vycor disk. The results of a new helium in Vycor experiment with a design that is completely free from any bulk solid shear modulus stiffening effect [81].

According to Anderson [76], "*Crystal defects enhance the local density of vacancies*". Observations are conjectured to be describable in terms of a rarified Gross–Pitaevskii superfluid of vacancies, with a transition temperature of about 50 mK, whose density is locally enhanced by crystal imperfections. The observations can be affected by this density enhancement. Therefore, disorder and defects that could enhance the local mass density appear to play an important yet uncertain role in the supersolidity of ^{4}He crystals [82].

The interatomic "bond" breaks easily for ^{4}He crystals, which requires energy at the critical point of 4.2 K for liquid–vapor transition in the order of 1/3,000 eV, much smaller than a typical van der Waals bond of 0.1 eV or around. The extremely weak interatomic interaction without charge sharing makes the ^{4}He atoms or grains are stickingless—more like hard spheres with closed electronic shell packing together. The stickingless interaction between grains will lower the friction coefficient.

The understanding of slipperiness of ice provides a mechanism for the superfluidity and supersolidity of ^{4}He crystal. Repulsion between the "electric monopoles locked in the elastic skins" of the small grains could resolve this puzzle. Broken-bond-induced local strain and quantum entrapment leads to a densification of charge and energy in the skin of a few atomic layers thick. The densification of energy corresponds to the enhancement of the elasticity, which stiffens the solid skin allowing the ^{4}He segment to react elastically to a shear stress. The repulsion between the densely entrapped electrons makes the motion frictionless. ^{4}He crystals lack the nonbonding electrons because of the close atomic shells. Therefore, the broken bonds that serve as not only centers that initiate structure failure but also provide sites for pinning dislocations by charge and energy entrapment, which could be responsible for the superfluidity and supersolidity as observed. Its "supersolid" behavior results just from

atomic CN imperfection that changes the bulk properties of the crystal [83]—Atomic undercoordination induces local quantum entrapment and polarization. Lattice contraction of the supersolid ^{4}He segments is expected to happen, though this contraction is tiny [63].

5.2 Superlubricity in dry sliding: Atomistic friction

The ultralow-friction linear bearing of carbon nanotubes (CNTs) and the superlubricity at dry nanocontacts sliding in high vacuum [84, 85] are fascinating. As shown in Fig. 15(a), the velocity of the liquid water moving in the CNTs is inversely proportional to the diameter under constant pressure applied to the CNT ends [86], which is beyond theory expectations. Transmission electron microscopy revealed that the inner walls of a multi-walled CNT can slide back and forth with respect to the outer walls of the CNT, being free from wear for all cycles of motion (see Fig. 15(b)) [87]. Surface energy calculations suggested that the force retracting the core nanotubes back into the outer tubes was 9 nN, being much lower than the van der Waals forces pulling the core nanotubes back into their sheath. The removal of the outer walls of the multi-walled CNT (MWCNT) corresponded to the highly localized dissipation at defect scattering sites, located primarily at the ends of the tube. The demonstration of ultralow friction between multi-walled CNT layers confirms that they will be useful mechanical components in molecular nanotechnology such as molecular bearing.

5.3 Quantum friction: charging and isotopic phonon effect

The occurrence of quantum friction is a kinetic process of energy dissipation ($E = f_r \cdot s$ with f_r being the friction force and s the sliding distance) due to the phonon (heat) and electron excitation (electron–hole pair production) during sliding [88]. A state of ultralow friction is reached when a sharp tip slides over a flat surface and the applied pressure is below a certain threshold, whose value is dependent on the surface potential sensed by the tip and the stiffness of the contacting materials [89–91].

A comparative study of hydrogen- and deuterium-terminated single-crystal diamond and silicon surfaces revealed that the hydrogenated surface (terminated with H^+) exhibited higher friction than the surface passivated with $^2H^+$, as illustrated in Fig. 16. The additional neutron in the $^2H^+$ plays a certain yet unclear role of significance because of the possible mass difference between the H and ^{2}H adsorbates [88]. In fact, adsorption of the isotope lowers the vibration frequency by $2^{-1/2}$ of the adsorbate on substrate by folding the reduced mass of the oscillator, which reduces the friction coefficient [36].

However, if changes the tip to ice sliding on ice with Deuterium addition, situation may reverse—the friction coefficient, or the shear strength of the O:D nonbond should be higher than that of the OH because

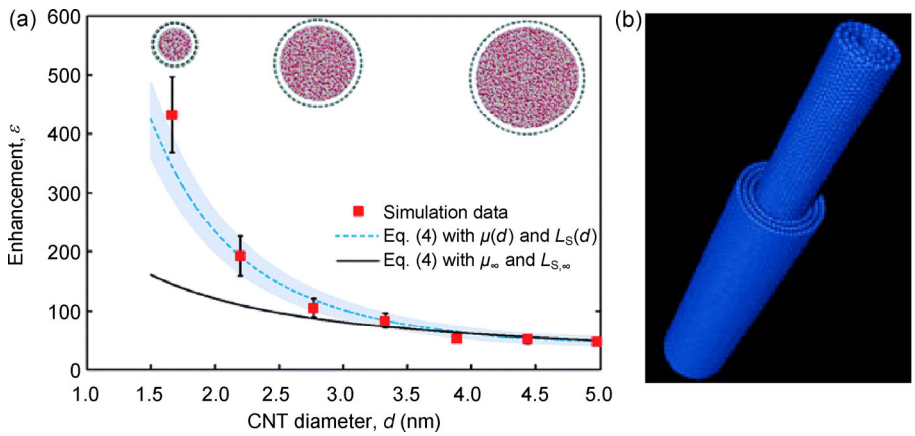

Fig. 15 (a) Superfluidity of water droplet in CNTs of different diameters [86] and (b) ultralow-friction nanoscale linear bearing made of multi-walled CNT [87].

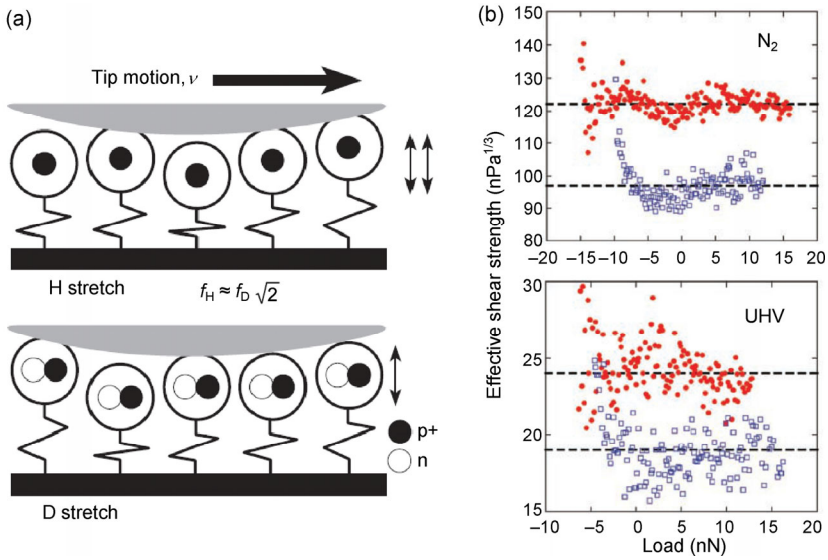

Fig. 16 (a) A schematic of the frictional interface. Vibrating adsorbates collide with and dissipate kinetic energy from the moving tip at a rate that depends on the adsorbate's frequency and thus its mass. (b) The shear strength of the H−C bond (red symbols) is higher than that of the D−C bond (blue symbols) measured in the N_2 and vacuum conditions (Reproduced with permission from Ref. [88], Copyright Science, 2007).

of the uncoupled resonance of the low-frequency and high-amplitude vibrations of the tip and substrate (see Section 4.7).

Park et al. [92] found a remarkable type and concentration dependence of the friction force on doped silicon. The friction force between the AFM sliding conductive TiN tip and the doped Si is substantially different, as given in Fig. 17. Charge depletion or accumulation on a Si substrate with patterned p and n stripes contributes differently to the friction force under a bias. A positive bias applied to the p-region causes a substantial increase of the friction force. If the n-region is biased positively, an accumulation of holes (+ charged) in the p-region. No variation of friction force was resolved between n and p regions under negative bias. Attraction between unlike charges or current flow will enhance the atomistic friction.

Both observations [88, 92] indicate clearly that the positively charged (H^+) tip or substrate (electronic holes +) would induce high friction force [23].

The superlubricity phenomenon was explained using the classical Prandtl–Tomlinson (PT) model [93, 94] and its extensions, including thermal activation, temporal and spatial variations of the surface corrugation, and multiple-contact effects [89]. Observation suggests that the friction force depends linearly on the number of atoms that interact chemically across

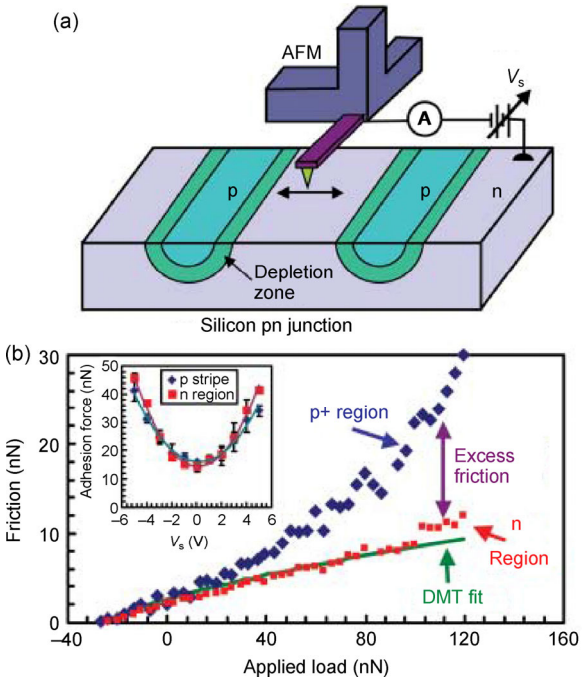

Fig. 17 (a) Schematic of AFM measurements on a silicon p-n junction device. (b) Plot of friction force as a function of applied load at +4 V sample bias. The inset shows the pull-off force as a function of sample bias (Reproduced with permission from Ref. [92], Copyright Science, 2006).

the contact [95]. According to the one-dimensional PT model, the slider atoms feel the periodic potential of the substrate surface atoms as they slide over them, experiencing a net force that is the sum of individual

instantaneous friction force on each atom resulting from the gradient of the periodic potential.

5.4 Solid lubrication due to nonbonding electron polarization

The mechanism of elastic interface Coulomb repulsion also applies to the frictionless CNT linear bearing and the superlubricity of micro channels. In fact, bond contraction happens to the CNT of limited number of walls. Bonds near the open ends contract even further [96]. Densification of the σ-bond electrons and polarization of the π-electrons take place to all the CNT walls; the repulsion between the densely packed and locally polarized like charges will reduce the friction force substantially, while the electrostatic forces of the additionally densely charged CNT ends may provide force for retracting motion and oscillation. The saturated potential barrier due to the skin charge entrapment of nanocontacts also provides a repulsion force between the contacts.

Skins of nitrides, oxides, and fluorides share the similarity of water and ice. Figure 18 illustrates the bonding rules for superlubricity of nitrides, oxides, and fluorides. The difference between these compounds is the number of lone pairs associated with each electronegative atom and their group symmetry and geometrical orientations. The key gradient of ice slippery is the presence of electron lone pairs and undercoordinated molecules. The O:H nonbond softening is associated with vibration amplitude enlargement and charge density elevation due to dual polarization. N reacts with a solid A skin preferring C_{3v} symmetry, such as fcc(111) and hcp(0001) planes [98]. The N atom is located in a place between the top two layers and the lone pair is directed into the substrate. The surface is hence networked with the smaller A^+ and the saturate bonded N^{3-} cores with densely packed electrons. Hence, the top skin layer is chemically inert as mechanical stronger and harder. Electrons in the saturated bond should be more stable compared with the otherwise unbonded electrons in the neutral host atoms.

When react with other electropositive atoms, the sp^3-orbital hybridization occurs with creation of the lone pairs that polarize the neighboring atoms becoming dipoles. There are four additional features in the valence band. The nonbonding lone pairs are responsible for the phononic elasticity-low vibration frequency and high amplitude. The localized anti-bonding dipoles stem the surface repulsivity.

The high intra-surface stress due to the ionic network could be responsible for the hardness of the top layer of a nitride. On the other hand, the N^{3-}–A^+ network at the surface is connected to the substrate mainly through the nonbonding lone pairs. The nonbonding interaction is rather weak (~0.1 eV per bond) compared with the original metallic bonds (~1.0 eV per bond) or the intra-surface ionic bond (2~3 eV per bond). The weak lone-pair interaction is highly elastic within a critical load at which the weak interaction will break. Therefore, the enhanced intra-layer strength makes a nitride usually harder (~20 GPa), and the weakened inter-layer bonding makes the nitride highly elastic and self-lubricate. This mechanism also

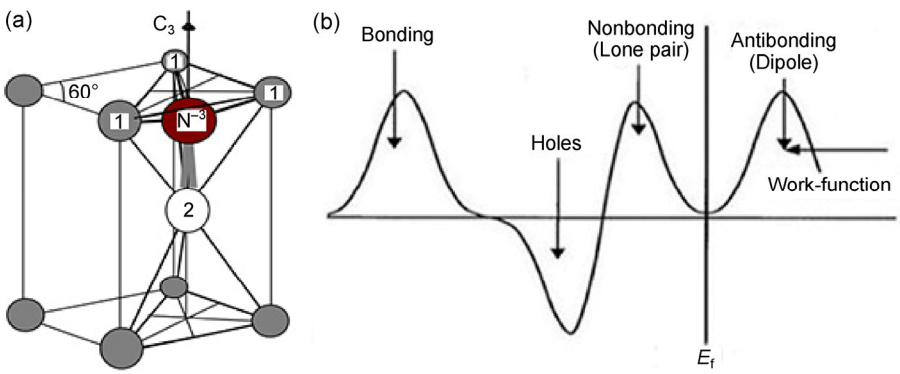

Fig. 18 (a) NB_4 nitride quasi-tetrahedron structure and (b) the associated valence density-of-states [97]. Smaller ions (labeled 1) donate electrons to the central N acceptor of which the sp orbits hybridize with production of a nonbonding lone pair (labeled 2). (b) N induced valence DOS with four features representing the states of bonding electron pairs, nonbonding lone pairs, antibonding dipoles, and electronic holes.

applies to graphite because of the weak π-nonbonding interaction along the [0001] direction.

Nanoindentation profiles from TiCrN surface and sliding friction measurements from CN and TiN surfaces have confirmed the predicted high elasticity and high hardness at lower pressing load and the existence of the critical scratching load [99]. As compared in Fig. 19(a), under 0.7 mN load of indentation, the elastic recoverability and hardness for a GaAlN film are higher than that of an amorphous carbon film [99]. The GaAlN surface is also much harder than the amorphous-C film under the lower indentation load. Figure 19(b) shows the profiles of pin-on-disk sliding friction test. The abrupt increase of the friction coefficient of nitride films represents the critical load. For polycrystalline diamond thin films, no such abruption in friction coefficient is observed though the friction coefficient is generally higher than nitride films. The absence of lone pairs in a-C film makes the film less elastic than a nitride film under the same pressing load. The abrupt change in the friction coefficient evidences the existence of critical load that breaks the nitride interlayer bonding-lone pair interaction. Therefore, the non-bonding interaction enhances the elasticity of nitride surfaces. Such high elasticity and high hardness by nature furnishes the nitride surfaces with self-lubricate for tribological applications.

The mechanism of slipperiness of ice is analogous to the self-lubrication of metal nitride [99, 100] and oxide [101] skins with electron lone pairs coming into play. TiCrN, GaAlN and α-Al_2O_3 skins exhibit a 100% elastic recovery at nanoindentation load under the critical friction load (e.g., <5 N for carbon nitride) at which the lone pair breaks.

Figure 20 shows the zone-selective electron spectrometrics (ZPS) profiles for Ti–O and Ti–N. The

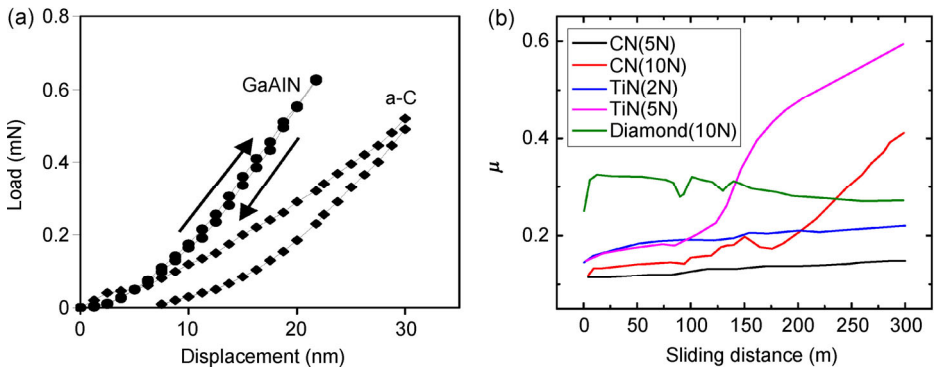

Fig. 19 Electron lone pairs serve as solid lubricants. (a) GaAlN/Al_2O_3 exhibits higher hardness and full elastic recoverability in comparison to amorphous carbon films under the same load. (b) The pin-on-disc measurements of the sliding friction coefficients of nitrides and diamond under different loads. Lowering the operating temperature from the ambient (b) may reduce nitrides' friction coefficient to be compatible to that of ice. The abrupt increase of the coefficient indicates the presence of the critical load at which the lone pair nonbond breaks (Reprinted with permission from Ref. [99] and references therein, Copyright AIP Publishing, 2001).

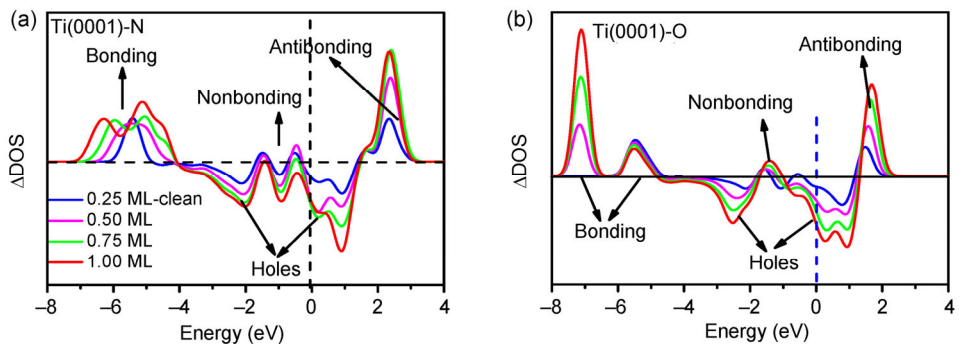

Fig. 20 Comparison (a) Ti(0001)-N with (b) Ti(0001)-O calculated ZPS profiles of n(Ti + X)−n(Ti), at 0.25, 0.50, 0.75, 1.00 ML with respect to that of clean Ti(0001) surface . Where n(Ti + X) is the DOS of the adsorbate system Ti(0001)–X (X = N, O), and n(Ti) the clean Ti(0001). Both reveal four DOS features corresponding to antibonding, nonbonding, bonding states and holes, which concur with the 3B prediction.

spectral difference between the chemisorbed surface and the clean reference show both oxide and nitride share the same valence DOS features as expected in Fig. 18. Raman spectra in Fig. 21 further evidence the presence of lone pairs in oxides and nitrides with character frequencies ranged below 1,000 cm^{-1}. However, carbon and carbide manifest no such features. The lone-pair features of oxides are stronger than those of nitrides, which result from the number of lone pairs of an oxygen and nitrogen atom.

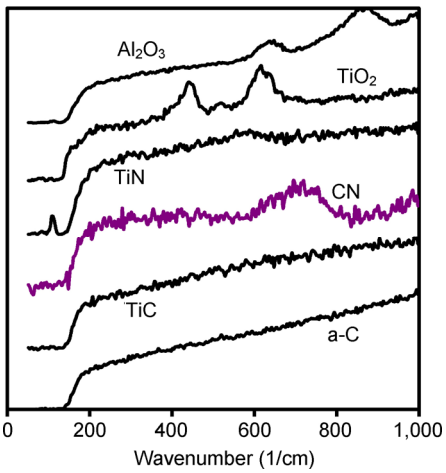

Fig. 21 Low-frequency Raman shifts indicate that non-bonding lone pair interaction exists in oxides and nitrides but carbides. Peak intensities of oxides are stronger than that of nitrides because of the number of the lone pairs that follow the 4-n rule (Reproduced with permission from Ref. [99], Copyright AIP Publishing, 2001).

6 Solution wet lubrication

In order to lower the friction coefficient at moving contacts, one often appeals to solute grease lubricant or detergent like graphite and sulfide powers. Little attention has been paid to the acid and alcohol solutions but a group of researchers at Tsinghua University has been focused on the mechanism of such solute lubricants. The following shows two excellent lubricants containing acids and alcohols that have ensured the superlubricity with extremely low friction coefficients. Electrification of the O:H–O bond by the excessive H^+ in the contacting interface and the molecular undercoordination induced skin supersolidity play significant roles in promoting the lubrication, according to the present knowledge. Readers may be referred to Ref. [102] for a comprehensive review on the fluid friction dynamics at the nanometer scale from the perspectives of diffusion, molecular cooperativity, and phase transition, during notion at the hydrophobic and hydrophilic interfaces.

6.1 Acid solutions

Phosphoric acid solutions exhibit superlubricity effect as a lubricant [103] with a friction coefficient around 0.004 after a short running-in period (Fig. 22). During sliding test, H^+ ions bond to the friction surfaces through tribochemical reaction, and meantime, the phosphoric acid and water molecules can form a stable

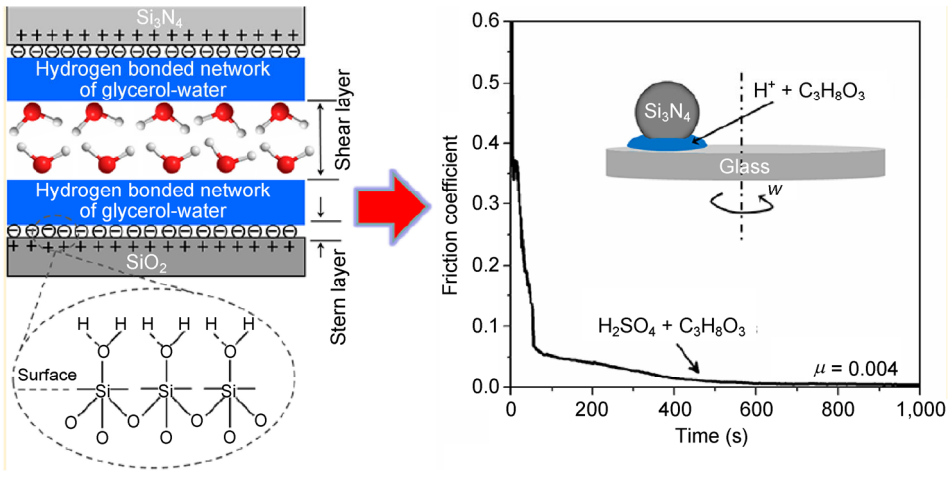

Fig. 22 Schematic of the experimental set up and the friction behavior of solution lubricants (acids or alcohols) that lowers the friction coefficient to 0.004 (Reproduced with permission from Ref. [105], Copyright ACS Publications, 2012).

hydrogen bonded network and then superlubricity appears [104]. The superlubricity of the aqueous acid arises from the polarization of the nonbonding electron lone pairs by H^+ ions that create local electric field. Ionic electrification will align, stretch, and polarize the O:H–O bond, which enhances the skin supersolidity. The ionic electrification and molecular undercoordination promote superlubricity of the acid solution. This is also true for saline ice [18].

6.2 Acids

The friction force between a silica particle and silica wafer changes with the lubricant of pure water and electrolyte solutions of LiCl, NaCl, and CsCl salts [106]. Figure 23 shows that smaller and more hydrated cations have higher lubrication capacities than the larger and less hydrated cations. Furthermore, the friction force also drops with the increases of solute concentration.

Observations agree with Raman phonon spectrometric results showing that the ionic electrification stiffens the H–O ω_H phonon in the order $Na^+ > K^+ > Rb^+ > Cs^+$ and the bulk ω_H shifts more significantly than those in the skin [7]. The ω_H blue shift is associated with the O:H ω_L softening. The phonon cooperative relaxation indicates the electrification shortens the H–O bond and meanwhile lengthens the O:H bond through O–O Coulomb repulsion and polarization. This bond and phonon relaxation takes place throughout the solution so the bulk ω_H shift more than it is in the skin. O:H–O bond electrification by the short fields of ions raises the viscoelasticity of the lubricant.

6.3 Glycerol and alcohols

Glycerol is another efficient medium that promotes hydrogen-bonded network lubricancy. Ma et al. [107] found that a mixture of glycerol and boric acid results in the superlubricity behavior. The adsorbed diglycerin borate and the hydration layer polarize water molecules acting as the lubricant in the contact region. Strikingly, addition of glycerol can promote the superlubricity of numerous acid solutions [105]. The ultra-low friction coefficient is closely related to the pH value of acid and the concentration of glycerol.

Furthermore, a replacement of glycerol with polyhydroxy, the same family of glycerol, can also raise the superlubricity of the lubricant [108]. Therefore, the hydrated water layer between the hydrogen-bonded networks of polyhydroxy alcohol and water molecules on the positively charged surfaces forms a promising kind of lubricant for wet friction applications—polarization of the electron lone pairs in the bond network seems to be very effective.

7 Summary

Molecular undercoordination-induced O:H–O bond relaxation and the enhanced nonbonding electron polarization and skin elasticity clarify the skin supersolidity of ice. Consistence between theory and observations clarifies the following bonding rules for

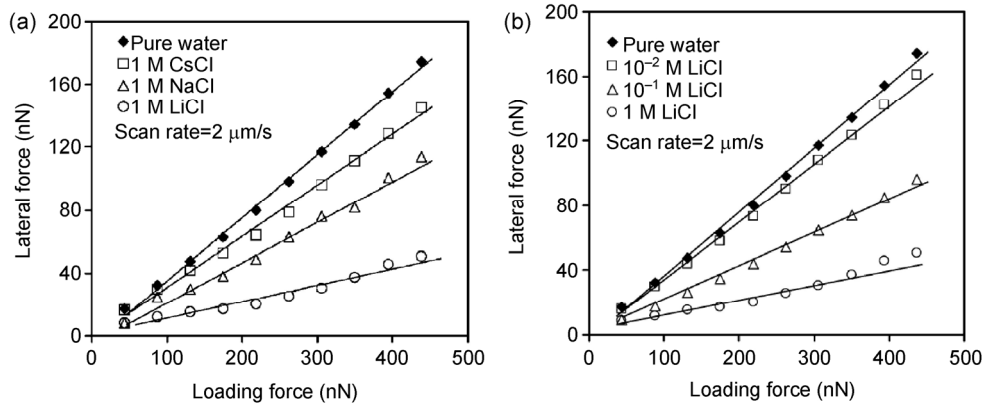

Fig. 23 Lateral force of a 6.8-μm silica particle interacting with a silica wafer using (a) H_2O, and CsCl, NaCl, and LiCl solutions of 1M at a fixed scan rate of 2 μm/s, and (b) its variation with the LiCl solution at 10^{-2}, 10^{-1}, and 1.0 M concentrations (Reproduced with permission from Ref. [106], Copyright ACS Publications, 2005).

the superlubricancy of ice, aqueous solutions, and sold self-lubrication:

(1) Undercoordination-induced O:H–O relaxation results in the supersolid phase that is elastic, hydrophobic, thermally more stable, and less dense, which dictates the unusual frictionless behaviour of ice skin.

(2) The dual polarization makes ice skin hydrophobic, viscoelastic, and frictionless. Interface Coulomb repulsion and elasticity is essential to lower the friction force.

(3) The supersolid skin causes slipperiness of ice through the elastic Coulomb-levitation mechanism. The elastic, soft O:H nonbond springs of low frequency and high amplitude of vibration attached with pinned dipoles have high recoverability of reformation.

(4) These understanding extend to the superfluidity of ^{4}He and the lubricity of water droplet flow in carbon nanotubes as well as nitrides and oxides.

(5) Lone pair interactions and the skin polarization play the key role in determining the dry and wet lubricity in lowering the friction coefficient.

The presence of phononic elasticity and electronic repulsivity is essential for superlubrication. Nonbond vibration creates soft phonons of low frequency and high magnitude with extraordinary recoverability of deformation. Localized polarization by the electron lone pairs and the densely entrapped core and bonding electrons provide the repulsivity at contacts. O:H–O bond electrification by charged ions would be an promising means for lowering the friction coefficient to realize superlubricancy.

Acknowledgement

Financial supports from the National Natural Science Foundation of China (Nos. 21273191 and 11502223) and inspiring discussion with Professor Ya-Pu Zhao are gratefully acknowledged.

References

[1] Faraday M. Note on regelation. *Proc R Soc London* **10**: 440–450 (1859)

[2] Thomson J. Note on Professor Faraday's recent experiments on regelation. *Proc R Soc London* **10**: 151–160 (1859)

[3] James T B. Melting and regelation of ice. *Nature* **5**: 185 (1872)

[4] Bowden F, Hughes T. The mechanism of sliding on ice and snow. *Proc Roy Soc London A* **172**(949): 280–298 (1939)

[5] Gurney C. Surface forces in liquids and solids. *Proc Roy Soc London A* **62**(358): 639–655 (1949)

[6] Krim J. Friction at the atomic scale. *Sci Am* **275**(4): 74–80 (1996)

[7] Sun Y, Sun C Q. *The Soul of Water: Single Notion, Multiple Myths*. Springer-Verlag, 2016.

[8] Liang H, Martin J M, Mogne T L. Experimental investigation of friction on low-temperature ice. *Acta Mater* **51**(9): 2639–2646 (2003)

[9] Sun C Q, Zhang X, Fu X, Zheng W, Kuo J-L, Zhou Y, Shen Z, and Zhou J. Density and phonon-stiffness anomalies of water and ice in the full temperature range. *J Phys Chem Lett* **4**: 3238–3244 (2013)

[10] Kietzig A-M, Hatzikiriakos S G, Englezos P. Physics of ice friction. *J Appl Phys* **107**(8): 081101–15 (2010)

[11] Zhang X, Huang Y, Ma Z, Zhou Y, Zheng W, Zhou J, Sun C Q. A common supersolid skin covering both water and ice. *Phys Chem Chem Phys* **16**(42): 22987–22994 (2014)

[12] Sun C Q, Zhang X, Zhou J, Huang Y, Zhou Y, Zheng W. Density, elasticity, and stability anomalies of water molecules with fewer than four neighbors. *J Phys Chem Lett* **4**: 2565–2570 (2013)

[13] Sun C Q. *Relaxation of the Chemical Bond*. Springer, 2014.

[14] Silvera Batista C A, Larson R G, Kotov N A. Nonadditivity of nanoparticle interactions. *Science* **350**(6257) (2015)

[15] Li J, Chen H, and Stone H A. Ice lubrication for moving heavy stones to the Forbidden City in 15th- and 16th-century China. *Proc Natl Acad Sci USA* **100**(50): 20023–20027 (2013)

[16] Krim J. Friction and energy dissipation mechanisms in adsorbed molecules and molecularly thin films. *Adv Phys* **61**(3): 155–323 (2012)

[17] Sukhorukov S, Loset S. Friction of sea ice on sea ice. *Cold Reg Sci Technol* **94**: 1–12 (2013)

[18] Kennedy F, Schulson E, Jones D. The friction of ice on ice at low sliding velocities. *Philos Mag A* **80**(5): 1093–1110 (2000)

[19] Schulson E M, Fortt A L. Friction of ice on ice. *J Geophys Res* **117**: B12204 (2012)

[20] Zhang X, Huang Y, Sun P, Liu X, Ma Z, Zhou Y, Zhou J, Zheng W, Sun C Q. Ice regelation: Hydrogen-bond extraordinary recoverability and water quasisolid-phase-boundary dispersivity. *Sci Rep* **5**: 13655 (2015)

[21] Rosenberg R. Why is ice slippery? *Phys Today* **58**(12): 50 (2005)

[22] Sun C Q. Size dependence of nanostructures: Impact of bond order deficiency. *Prog Solid State Chem* **35**(1): 1–159 (2007)

[23] Strelcov E, Kumar R, Bocharova V, Sumpter B G, Tselev A, Kalinin S V. Nanoscale lubrication of ionic surfaces controlled via a strong electric field. *Sci Rep* **5**: 8049 (2015)

[24] Orem M W, Adamson A W. Physical adsorption of vapor on ice: II. n-alkanes. *J Colloid Interf Sci* **31**(2): 278–286 (1969)

[25] Molina M J. Heterogeneous chemistry on polar stratospheric clouds. *Atmos Environ A* **25**(11): 2535–2537 (1991)

[26] Kvlividze V I, Kiselev V F, Kurzaev A B, Ushakova L A. The mobile water phase on ice surfaces. *Surf Sci* **44**(1): 60–68 (1974)

[27] Golecki I, Jaccard C. The surface of ice near 0 ˚C studied by 100 keV proton channeling. *Phys Lett A* **63**(3): 374–376 (1977)

[28] Furukawa Y, Yamamoto M, Kuroda T. Ellipsometric study of the transition layer on the surface of an ice crystal. *J Cryst Growth* **82**(4): 665–677 (1987)

[29] Dosch H, Lied A, Bilgram J H. Glancing-angle X-ray scattering studies of the premelting of ice surfaces. *Surf Sci* **327**(1–2): 145–164 (1995)

[30] Li Y, Somorjai G A. Surface premelting of ice. *J Phys Chem C* **111**(27): 9631–9637 (2007)

[31] Döppenschmidt A, Butt H-J. Measuring the thickness of the liquid-like layer on ice surfaces with atomic force microscopy. *Langmuir* **16**(16): 6709–6714 (2000)

[32] Engemann S, Reichert H, Dosch H, Bilgram J, Honkimaki V, Snigirev A. Interfacial melting of ice in contact with SiO_2. *Phys Rev Lett* **92**(20): 205701 (2004)

[33] Sun C Q, Sun Y, Ni Y G, Zhang X, Pan J S, Wang X H, Zhou J, Li L T, Zheng W T, Yu S S, Pan L K, Sun Z. Coulomb repulsion at the nanometer-sized contact: A force driving superhydrophobicity, superfluidity, superlubricity, and supersolidity. *J Phys Chem C* **113**(46): 20009–20019 (2009)

[34] Sun C Q, Zhang X, Zheng W T. Hidden force opposing ice compression. *Chem Sci* **3**: 1455–1460 (2012)

[35] Huang Y, Zhang X, Ma Z, Zhou Y, Zhou J, Zheng W, Sun C Q. Size, separation, structure order, and mass density of molecules packing in water and ice. *Sci Rep* **3**: 3005 (2013)

[36] Huang Y, Zhang X, Ma Z, Zhou Y, Zheng W, Zhou J, Sun C Q. Hydrogen-bond relaxation dynamics: Resolving mysteries of water ice. *Coord Chem Rev* **285**: 109–165 (2015)

[37] Liu X J, Bo M L, Zhang X, Li L T, Nie Y G, Tian H, Sun Y, Xu S, Wang Y, Zheng W, Sun C Q. *Coordination-resolved electron spectrometrics*. Chem. Rev. **115**(14): 6746–6810 (2015).

[38] Zhang J, Chen P, Yuan B, Ji W, Cheng Z, and Qiu X, Real-space identification of intermolecular bonding with atomic force microscopy. *Science* **342**(6158): 611–614 (2013)

[39] Wilson K R, Schaller R D, Co D T, Saykally R J, Rude B S, Catalano T, Bozek J D. Surface relaxation in liquid water and methanol studied by x-ray absorption spectroscopy. *J Chem Phys* **117**(16): 7738–7744 (2002)

[40] Kahan T F, Reid J P, Donaldson D J. Spectroscopic probes of the quasi-liquid layer on ice. *J Phys Chem A* **111**(43): 11006–11012 (2007)

[41] Sulpizi M, Salanne M, Sprik M, Gaigeot M-P. Vibrational sum frequency generation spectroscopy of the water liquid–vapor interface from density functional theory-based molecular dynamics simulations. *J Phys Chem Lett* **4**(1): 83–87 (2013)

[42] Abu-Samha M, Borve K J, Winkler M, Harnes J, Saethre L J, Lindblad A, Bergersen H, Ohrwall G, Bjorneholm O, Svensson S. The local structure of small water clusters: Imprints on the core-level photoelectron spectrum. *J Phys B* **42**(5): 055201 (2009)

[43] Nishizawa K, Kurahashi N, Sekiguchi K, Mizuno T, Ogi Y, Horio T, Oura M, Kosugi N, Suzuki T. High-resolution soft X-ray photoelectron spectroscopy of liquid water. *Phys Chem Chem Phys* **13**: 413–417 (2011)

[44] Winter B, Aziz E F, Hergenhahn U, Faubel M, Hertel I V. Hydrogen bonds in liquid water studied by photoelectron spectroscopy. *J Chem Phys* **126**(12): 124504 (2007)

[45] Harich S A, Hwang D W H, Yang X, Lin J J, Yang X, Dixon R N. Photodissociation of H_2O at 121.6 nm: A state-to-state dynamical picture. *J Chem Phys* **113**(22): 10073–10090 (2000)

[46] Uysal A, Chu M, Stripe B, Timalsina A, Chattopadhyay S, Schlepütz C M, Marks T J, Dutta P. What x rays can tell us about the interfacial profile of water near hydrophobic surfaces. *Phys Rev B* **88**(3): 035431 (2013)

[47] Hammer N I, Shin J W, Headrick J M, Diken E G, Roscioli J R, Weddle G H, Johnson M A. How do small water clusters bind an excess electron? *Science* **306**(5696): 675–679 (2004)

[48] Marsalek O, Uhlig F, Frigato T, Schmidt B, Jungwirth P. Dynamics of electron localization in warm versus cold water clusters. *Phys Rev Lett* **105**(4): 043002 (2010)

[49] Liu S, Luo J, Xie G, Guo D. Effect of surface charge on water film nanoconfined between hydrophilic solid surfaces. *J Appl Phys* **105**(12): 124301–4 (2009)

[50] Siefermann K R, Liu Y, Lugovoy E, Link O, Faubel M, Buck U, Winter B, Abel B. Binding energies, lifetimes and implications of bulk and interface solvated electrons in water. *Nat Chem* **2**: 274–279 (2010)

[51] Paik D H, Lee I R, Yang D S, Baskin J S, Zewail A H. Electrons in finite-sized water cavities: hydration dynamics observed in real time. *Science* **306**(5696): 672–675 (2004)

[52] Verlet J R R, Bragg A E, Kammrath A, Cheshnovsky O, Neumark D M. Observation of large water-cluster anions with surface-bound excess electrons. *Science* **307**(5706): 93–96 (2005)

[53] Vacha R, Marsalek O, Willard A P, Bonthuis D J, Netz R R, Jungwirth P. Charge transfer between water molecules as the possible origin of the observed charging at the surface of pure water. *J Phys Chem Lett* **3**(1): 107–111 (2012)

[54] Baletto F, Cavazzoni C, Scandolo S. Surface trapped excess electrons on ice. *Phys Rev Lett* **95**(17): 176801 (2005)

[55] Turi L, Sheu W S, Rossky P J. Characterization of excess electrons in water-cluster anions by quantum simulations. *Science* **309**(5736): 914–917 (2005)

[56] Zhang X, Sun P, Huang Y, Ma Z, Liu X, Zhou J, Zheng W, Sun C Q. Water nanodroplet thermodynamics: Quasi-solid phase-boundary dispersivity. *J Phys Chem B* **119**(16): 5265–5269 (2015)

[57] Qiu H, Guo W. Electromelting of confined monolayer ice. *Phys Rev Lett* **110**(19): 195701 (2013)

[58] Li J, Li Y X, Yu X, Ye W J, Sun C Q. Local bond average for the thermally driven elastic softening of solid specimens. *J Phys D-Appl Phys* **42**(4): 045406 (2009)

[59] Holmes M J, Parker N G, Povey M J W. Temperature dependence of bulk viscosity in water using acoustic spectroscopy. *J Phys: Conf Ser* **269**: 012011 (2011)

[60] Xu D, Liechti K M, Ravi-Chandar K. Mechanical probing of icelike water monolayers. *Langmuir* **25**(22): 12870–12873 (2009).

[61] Jinesh K B, Frenken J W M. Experimental evidence for ice formation at room temperature. *Phys Rev Lett* **101**(3): 036101 (2008)

[62] Kim E, Chan M H W. Probable observation of a supersolid helium phase. *Nature* **427**(6971): 225–227 (2004)

[63] Balibar S, Caupin F. Supersolidity and disorder. *J Phys: Condens Matter* **20**(17): 173201 (2008)

[64] Hunt B, Pratt E, Gadagkar V, Yamashita M, Balatsky A V, Davis J C. Evidence for a superglass state in solid ^{4}He. *Science* **324**: 632–636 (2009)

[65] Wang C, Lu H, Wang Z, Xiu P, Zhou B, Zuo G, Wan R, Hu J, Fang H. Stable liquid water droplet on a water monolayer formed at room temperature on ionic model substrates. *Phys Rev Lett* **103**(13): 137801–137804 (2009)

[66] James M, Darwish T A, Ciampi S, Sylvester S O, Zhang Z M, Ng A, Gooding J J, Hanley T L. Nanoscale condensation of water on self-assembled monolayers. *Soft Matter* **7**(11): 5309–5318 (2011)

[67] Ishiyama T, Takahashi H, Morita A. Origin of vibrational spectroscopic response at ice surface. *J Phys Chem Lett* **3**: 3001–3006 (2012)

[68] Sun C Q. Oxidation electronics: Bond-band-barrier correlation and its applications. *Prog Mater Sci* **48**(6): 521–685 (2003)

[69] Guo J, Meng X, Chen J, Peng J, Sheng J, Li X-Z, Xu L, Shi J-R, Wang E, Jiang Y. Real-space imaging of interfacial water with submolecular resolution. *Nat Mater* **13**: 184–189 (2014)

[70] Bluhm H, Inoue T, Salmeron M. Friction of ice measured using lateral force microscopy. *Phys Rev B* **61**(11): 7760 (2000)

[71] Andreev A, Lifshits I. Quantum theory of defects in crystals. *Zhur Eksper Teoret Fiziki* **56**(6): 2057–2068 (1969)

[72] Schindler T L. A possible new form of 'supersolid' matter national science foundation news. http://www.nsf.gov/news/news_videos.jsp?org=NSF&cntn_id=100323&preview=false&media_id=51151, 2005.

[73] Kim E, Chan M H. Observation of superflow in solid helium. *Science* **305**(5692): 1941–1944 (2004)

[74] Day J, Beamish J. Low-temperature shear modulus changes in solid He-4 and connection to supersolidity. *Nature* **450**(7171): 853–856 (2007)

[75] Balibar S. Supersolid helium: Stiffer but flowing. *Nat Phys* **5**(8): 534–535 (2009)

[76] Anderson P W. A gross-pitaevskii treatment for supersolid helium. *Science* **324**: 631–632 (2009)

[77] Pollet L, Boninsegni M, Kuklov A B, Prokof'ev N V, Svistunov B V, Troyer M. Local stress and superfluid properties of solid He-4. *Phys Rev Lett* **101**(9): 097202 (2008)

[78] Sasaki S, Ishiguro R, Caupin F, Maris H J, Balibar S. Superfluidity of grain boundaries and supersolid behavior. *Science* **313**(5790): 1098–1100 (2006)

[79] Maris H J. Effect of elasticity on torsional oscillator experiments probing the possible supersolidity of helium. *Phys Rev B* **86**(2): 020502 (2012)

[80] Kim D Y, Chan M H W. Absence of supersolidity in solid helium in porous vycor glass. *Phys Rev Lett* **109**(15): 155301 (2012)

[81] Kim D Y, Chan M H W. Upper limit of supersolidity in solid helium. *Phys Rev B* **90**(6): 064503 (2014)

[82] Saunders J. A glassy state of supersolid helium. *Science* **324**: 601–602 (2009)

[83] Dorsey A T, Huse D A. Condensed-matter physics: Shear madness. *Nature* **450**(7171): 800–801 (2007)

[84] Socoliuc A, Gnecco E, Maier S, Pfeiffer O, Baratoff A, Bennewitz R, Meyer E. Atomic-scale control of friction by actuation of nanometer-sized contacts. *Science* **313**(5784): 207–210 (2006)

[85] Gnecco E, Maier S, Meyer E. Superlubricity of dry nano-contacts. *J Phys-Condensed Matter* **20**(35): 354004 (2008)

[86] Thomas J A, McGaughey A J H. Reassessing fast water transport through carbon nanotubes. *Nano Lett* **8**(9): 2788–2793 (2008)

[87] Cumings J, Zettl A. Low-friction nanoscale linear bearing realized from multiwall carbon nanotubes. *Science* **289**(5479): 602–604 (2000)

[88] Cannara R J, Brukman M J, Cimatu K, Sumant A V, Baldelli S, Carpick R W. Nanoscale friction varied by isotopic shifting of surface vibrational frequencies. *Science* **318**(5851): 780–783 (2007)

[89] Socoliuc A, Bennewitz R, Gnecco E, Meyer E. Transition from stick-slip to continuous sliding in atomic friction: Entering a new regime of ultralow friction. *Phys Rev Lett* **92**(13): 134301 (2004)

[90] Erdemir A, Martin J M Eds. *Superlubricity*. Elsevier, 2007.

[91] Yuan Q Z, Zhao Y P. Hydroelectric voltage generation based on water-filled single-walled carbon nanotubes. *J Am Chem Soc* **131**(18): 6374–6376 (2009)

[92] Park J Y, Ogletree D F, Thiel P A, Salmeron M. Electronic control of friction in silicon pn junctions. *Science* **313**(5784): 186–186 (2006)

[93] Tomlinson G. CVI. A molecular theory of friction. *The London, Edinburgh, and Dublin Philosophical Magazine and Journal of Science* **7**(46): 905–939 (1929)

[94] Prandtl L. Mind model of the kinetic theory of solid bodies. *Z Ang Math Mech* **8**: 85–106 (1928)

[95] Mo Y F, Turner K T, Szlufarska I. Friction laws at the nanoscale. *Nature* **457**(7233): 1116–1119 (2009)

[96] Sun C Q, Bai H L, Tay B K, Li S, Jiang E Y. Dimension, strength, and chemical and thermal stability of a single C–C bond in carbon nanotubes. *J Phys Chem B* **107**(31): 7544–7546 (2003)

[97] Sun C Q. *A model of bonding and band-forming for oxides and nitrides*. *Appl Phys Lett* **72**(14): 1706–1708 (1998)

[98] Zheng W T, Sun C Q. Electronic process of nitriding: Mechanism and applications. *Prog Solid State Chem* **34**(1): 1–20 (2006)

[99] Sun C Q, Tay B K, Lau S P, Sun X W, Zeng X T, Li S, Bai H L, Liu H, Liu Z H, Jiang E Y. Bond contraction and lone pair interaction at nitride surfaces. *J Appl Phys* **90**(5): 2615–2617 (2001)

[100] Sun C Q. Thermo-mechanical behavior of low-dimensional systems: The local bond average approach. *Prog Mater Sci* **54**(2): 179–307 (2009)

[101] Lu C, Mai Y W, Tam P L, Shen Y G. Nanoindentation-induced elastic-plastic transition and size effect in α-Al_2O_3(0001). *Philos Mag Lett* **87**(6): 409–415 (2007)

[102] Zhao Y P. *Physical Mechanics of Surface and Interface*. Beijing: Science Press, 2012.

[103] Li J, Zhang C, Luo J. Superlubricity behavior with phosphoric acid-water network induced by rubbing. *Langmuir* **27**(15): 9413–9417 (2011)

[104] Li J, Zhang C, Sun L, Lu X, Luo J. Tribochemistry and superlubricity induced by hydrogen ions. *Langmuir* **28**(45): 15816–15823 (2012)

[105] Li J, Zhang C, Ma L, Liu Y, Luo J. Superlubricity achieved with mixtures of acids and glycerol. *Langmuir* **29**(1): 271–275 (2012)

[106] Donose B C, Vakarelski I U, Higashitani K. Silica surfaces lubrication by hydrated cations adsorption from electrolyte solutions. *Langmuir* **21**(5): 1834–1839 (2005)

[107] Ma Z-Z, Zhang C-H, Luo J-B, Lu X-C, Wen S-Z. Superlubricity of a mixed aqueous solution. *Chin Phys Lett* **28**(5): 056201 (2011)

[108] Li J, Zhang C, Luo J. Superlubricity achieved with mixtures of polyhydroxy alcohols and acids. *Langmuir* **29**(17): 5239–5245 (2013)

Xi ZHANG. She received her PhD degree in 2012 at Nanyang Technological University, Singapore, with research focus on developing the ZPS-TB algorithm and DFT-TB computing graphene edges, metallic nanocrystals, water and ice. She is now focusing on quantum friction and atomistic tribology.

Yongli HUANG. She received her PhD degree in 2013 at Xiangtan University, China, with research focus on probing hydrogen bond asymmetrical potentials using Lagrangian oscillating dynamics, and solid surface and interface mechanics.

Zengsheng MA. He obtained his PhD degree at Xiangtan University in 2011 with research interest in the physical-mechanical properties of low-dimensional and functional materials.

Lengyuan NIU. He received his PhD degree in 2013 from Lanzhou Institute of Chemical Physics with a research focus on colloid and interface chemistry.

Chang Qing SUN. He received his PhD degree in 1996 at Murdoch University, Australia, with research focus on undercoordination physics and heterocoordination chemistry. He has authored *Relaxation of the Chemical Bond* (Springer, 2014), *The Soul of Water* (Springer, 2016), and *Atomistic Bond-Electron-Phonon Spectrometrics* (communicated) in addition to treatises published in *Chem Rev* (2015 and 2012), *Coord Chem Rev* (2015), *Prog Solid State Chem* (2015, 2007, and 2006), *Surf Sci Rep* (2013), *Sci China* (2012), *Energy Environ Sci* (2011), *Nanoscale* (2010), *Prog Mater Sci* (2009 and 2003), etc.